Equilibrium and Dynamics of Remnants of Binary Neutron Star Mergers

NIKOLAOS STERGIOULAS

DEPARTMENT OF PHYSICS

ARISTOTLE UNIVERSITY OF THESSALONIKI

VIRGO

EUROPEAN COOPERATION IN SCIENCE & TECHNOLOGY

grnet

11th Iberian GW Meeting, June 10, 2021

GW170817 BINARY NEUTRON STAR MERGER

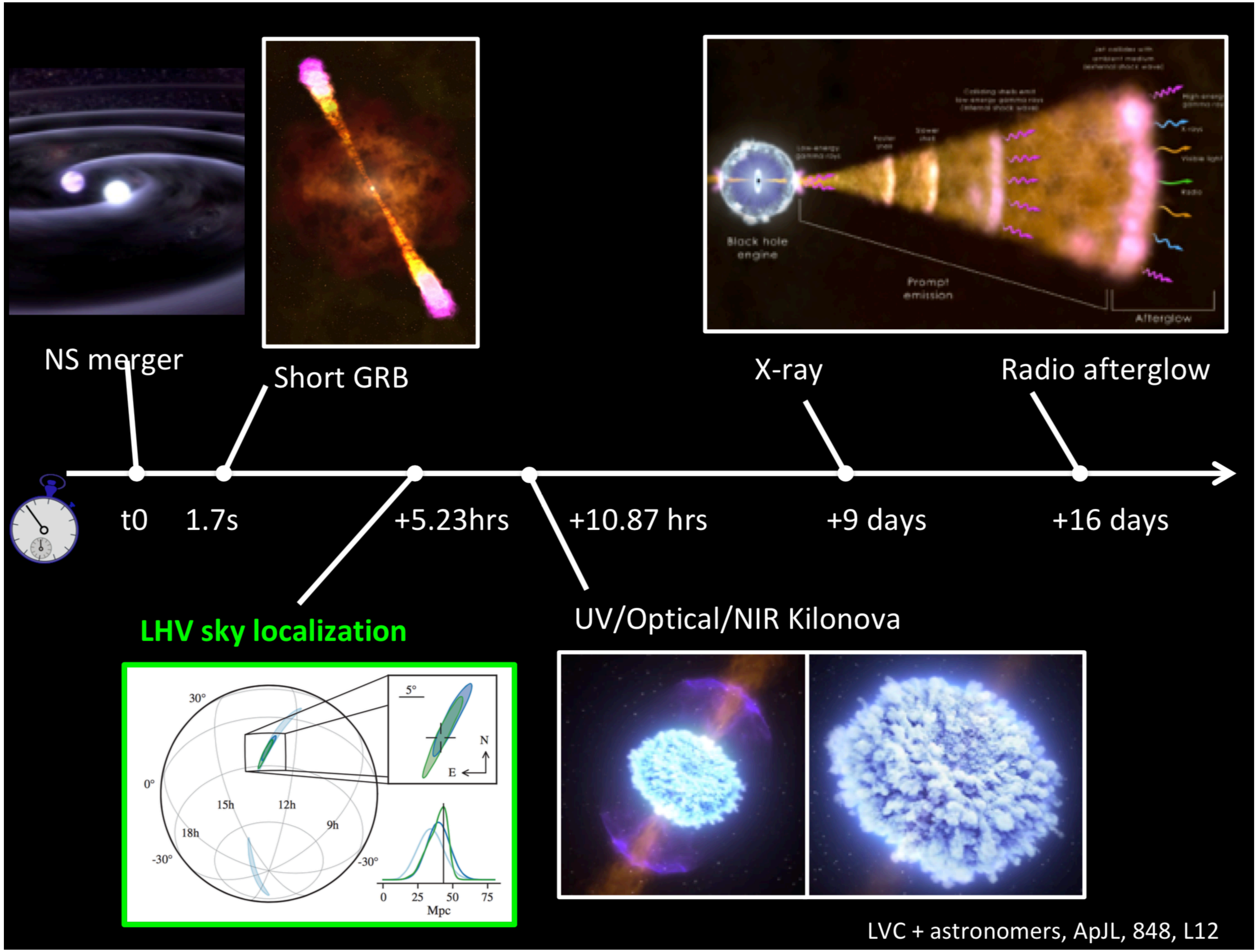

M. Branchesi

PLANNED OBSERVATIONS FOR THE NEXT FEW YEARS

Next observing run: O4 (starting date ~ summer 2022)

We may expect

$$10^{+52}_{-10}$$

BNS detections with the HLVK network.

O5 may reach ~2 x further, or ~8 x volume

Abbott et al. LRR (2020)

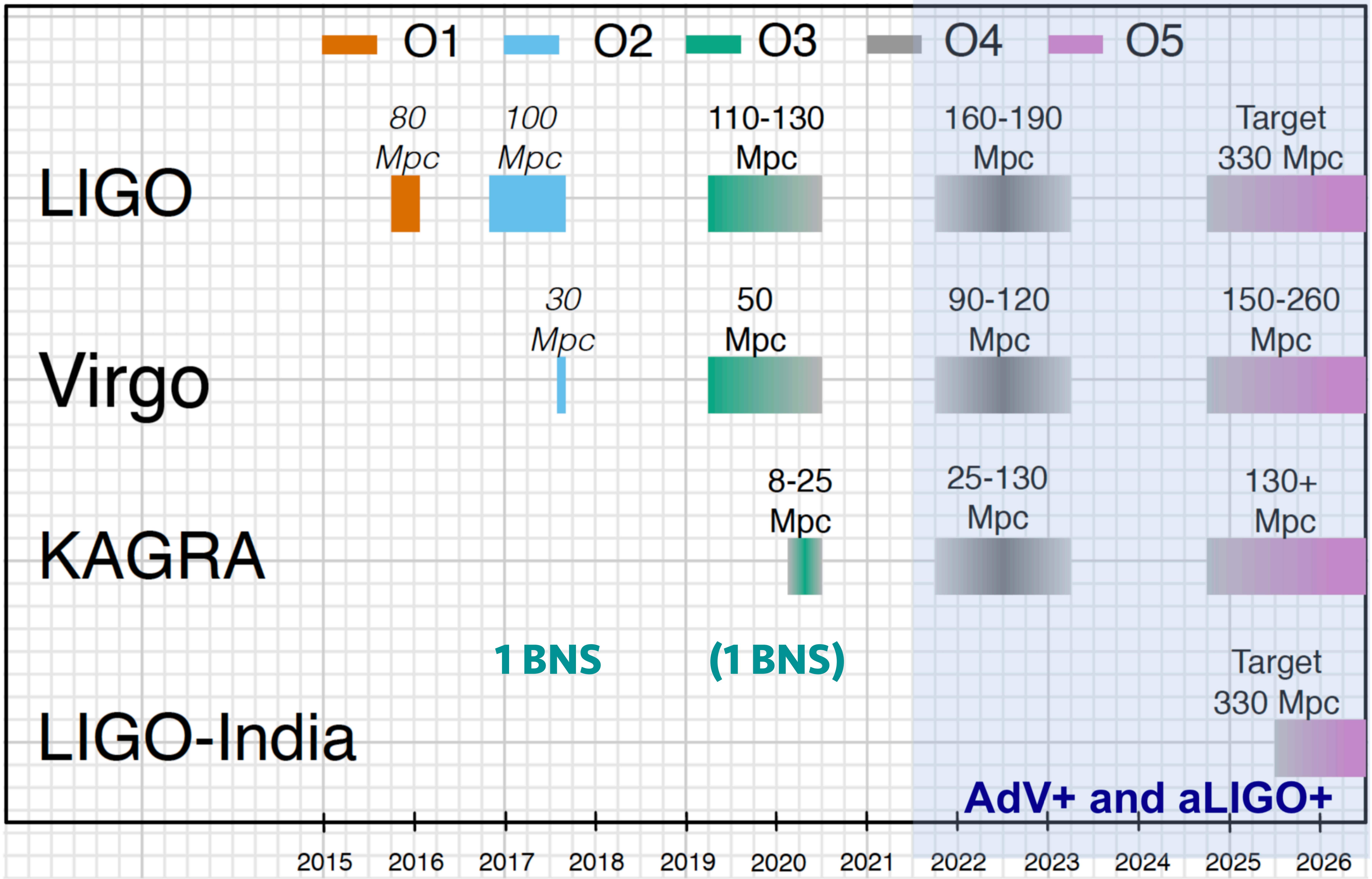

DETECTION EFFICIENCY OF BNS MERGERS WITH 3G DETECTORS

Detection efficiency of BNS mergers with various networks of 3G detectors.

(Assuming a population randomly oriented and located in space and detection SNR of 8.)

Rosati et al. arxiv2104.09535 (2021)

Joint GW + sGRB detections with THESEUS: up to *a few tens per year* (inl. aligned and misaligned jet w.r.t. the observer)

Ciolfi et al. arxiv2104.09534 (2021)

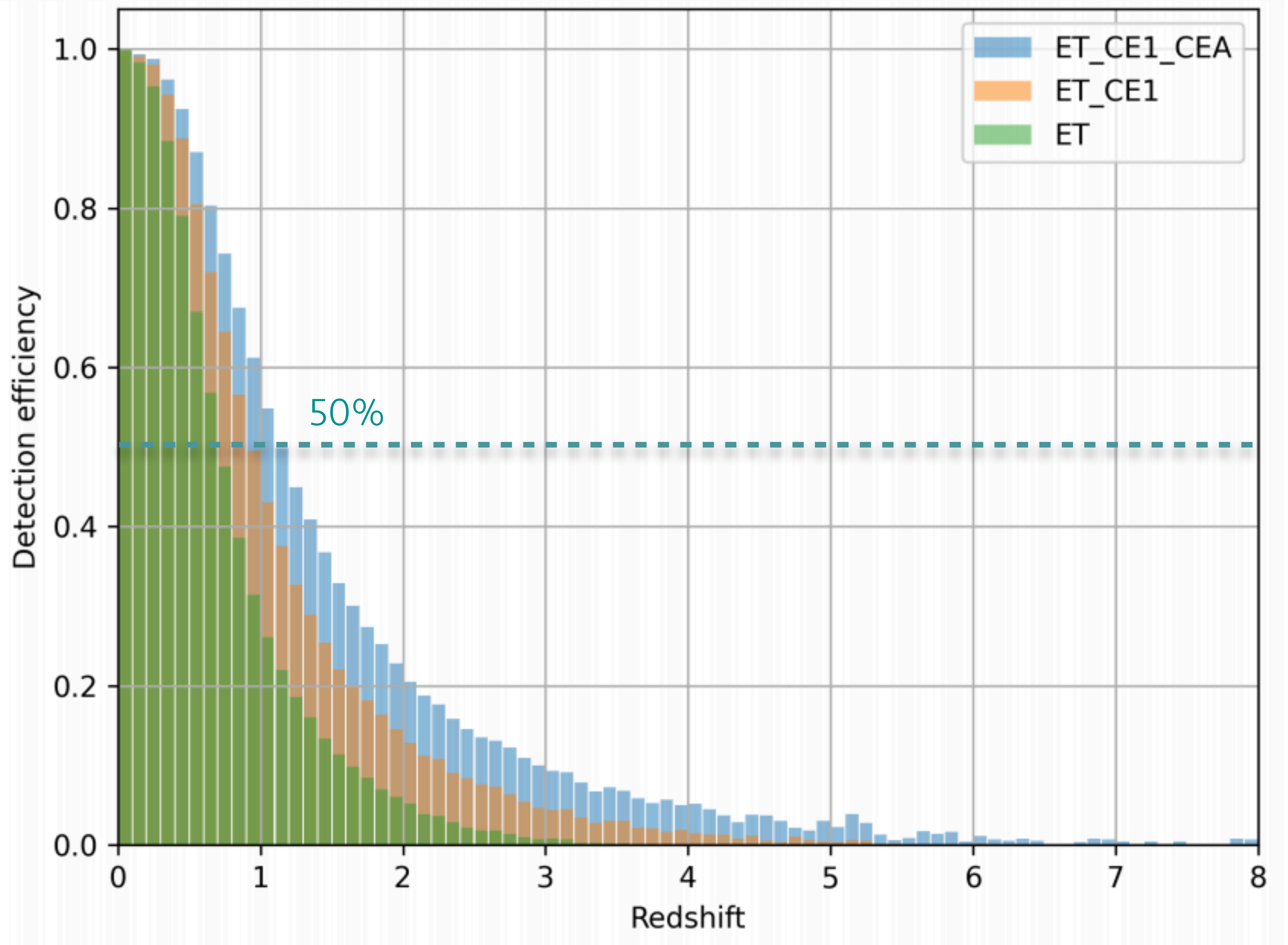

POSSIBLE OUTCOMES OF BNS MERGERS

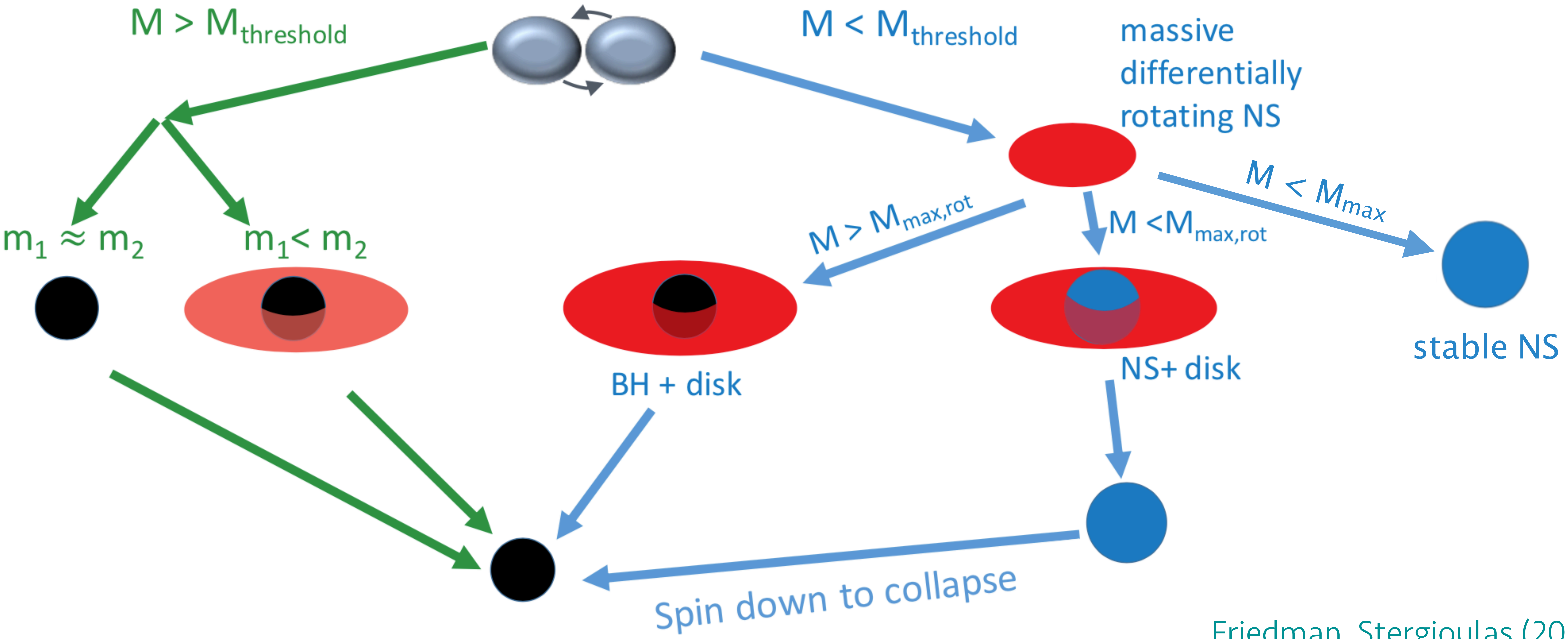

Friedman, Stergioulas (2020)

Significant differences in post-merger E/M emission, depending on the outcome of BNS mergers

The accurate determination of M_{thres} is important for GW and multi-messenger astronomy.

THRESHOLD MASS TO PROMPT COLLAPSE

Simulations with SPH+CFC code in GR:

- Equal mass mergers
- 12 fully temperature-dependent EOS
- 340k SPH particles

Empirical relation for the threshold mass to prompt collapse, in terms of the maximum TOV mass and the radius of 1.6 $M_\odot$ stars:

$$M_{\rm thres} = \left(-3.606\frac{GM_{\rm max}}{c^2 R_{1.6}} + 2.38\right)\cdot M_{\rm max}$$

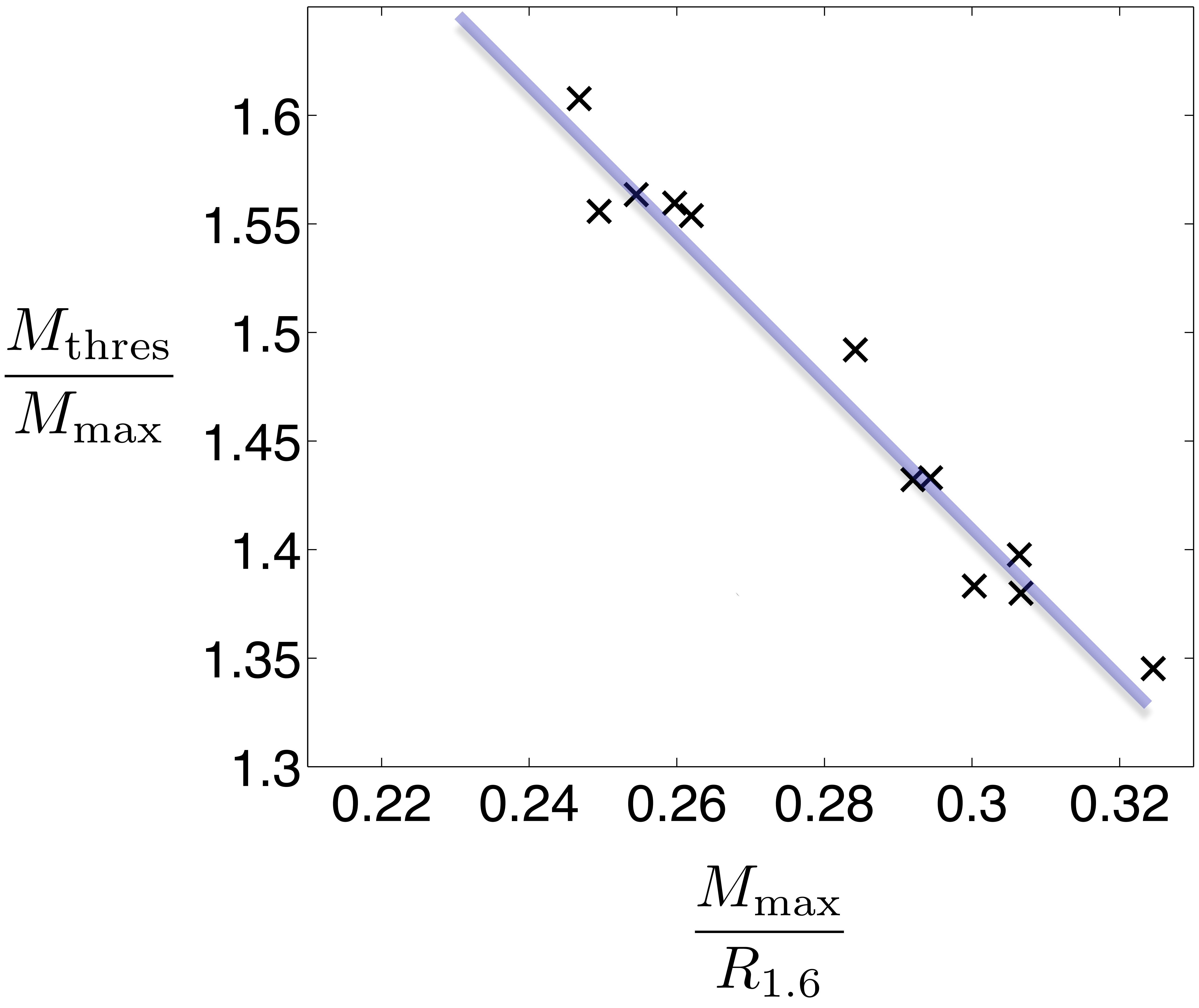

Bauswein, Baumgarte, Janka (2013)

EXTENSION OF EMPIRICAL RELATION FOR THRESHOLD MASS

Extended set of simulations with SPH+CFC code in GR:

- 33 hadronic EOS (fully temperature dependent or with an added thermal part)
- Mass ratio $0.7 \leq q \leq 1$
- Threshold mass determined within $0.025 M_\odot$

New, bilinear empirical relations of the form

$$M_{\rm thres}\,(M_\odot) = aM_{\rm max} + bR_{1.6} - c$$

or

$$M_{\rm thres}\,(M_\odot) = aM_{\rm max} + b\Lambda_{1.4} - c$$

Bauswein et al. (2021)

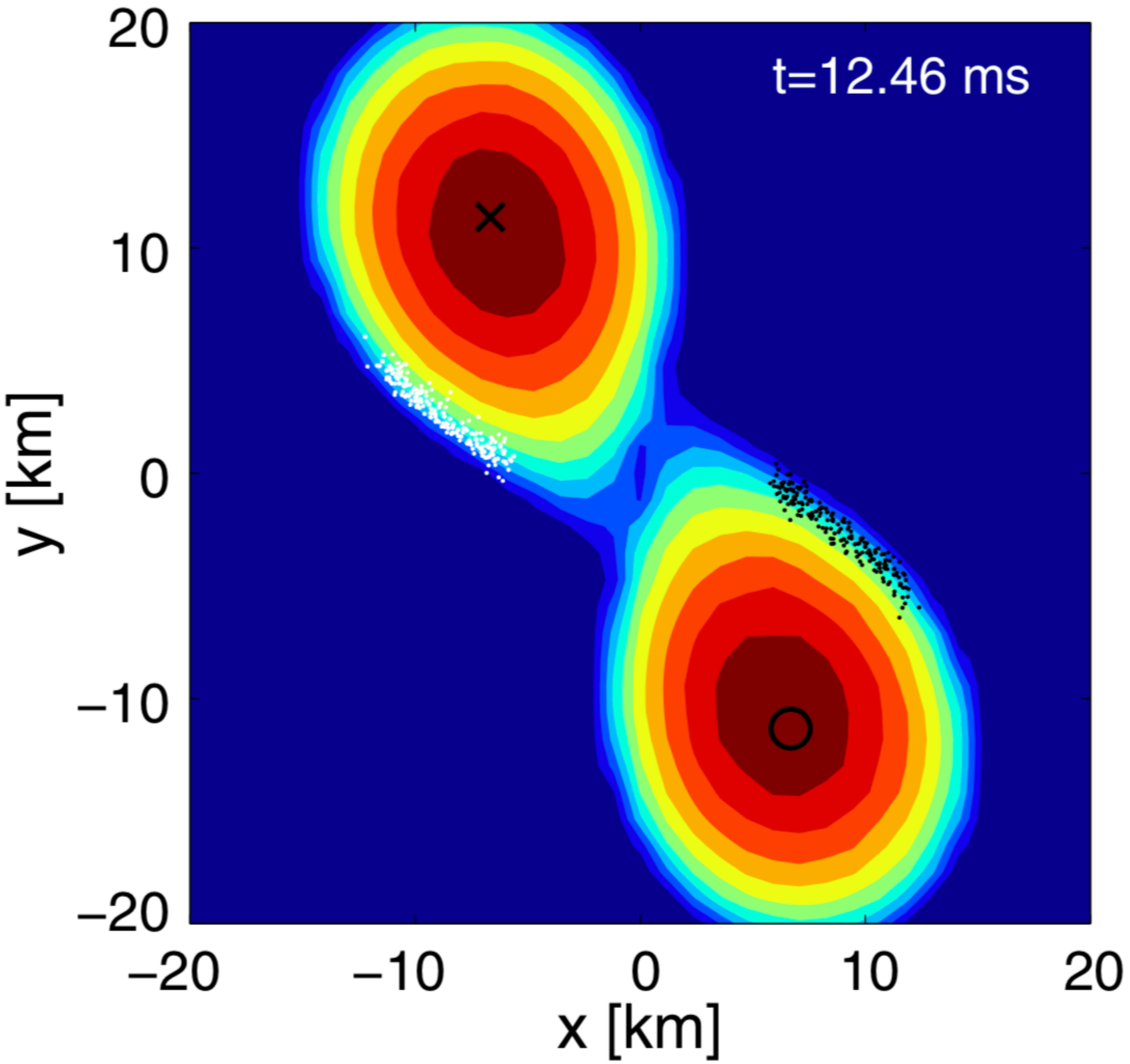

THRESHOLD MASS TO PROMPT COLLAPSE FOR DIFFERENT MASS RATIOS

New bilinear empirical relations of the form $M_{\rm thres} = aM_{\rm max} + bR_{1.6} + c$

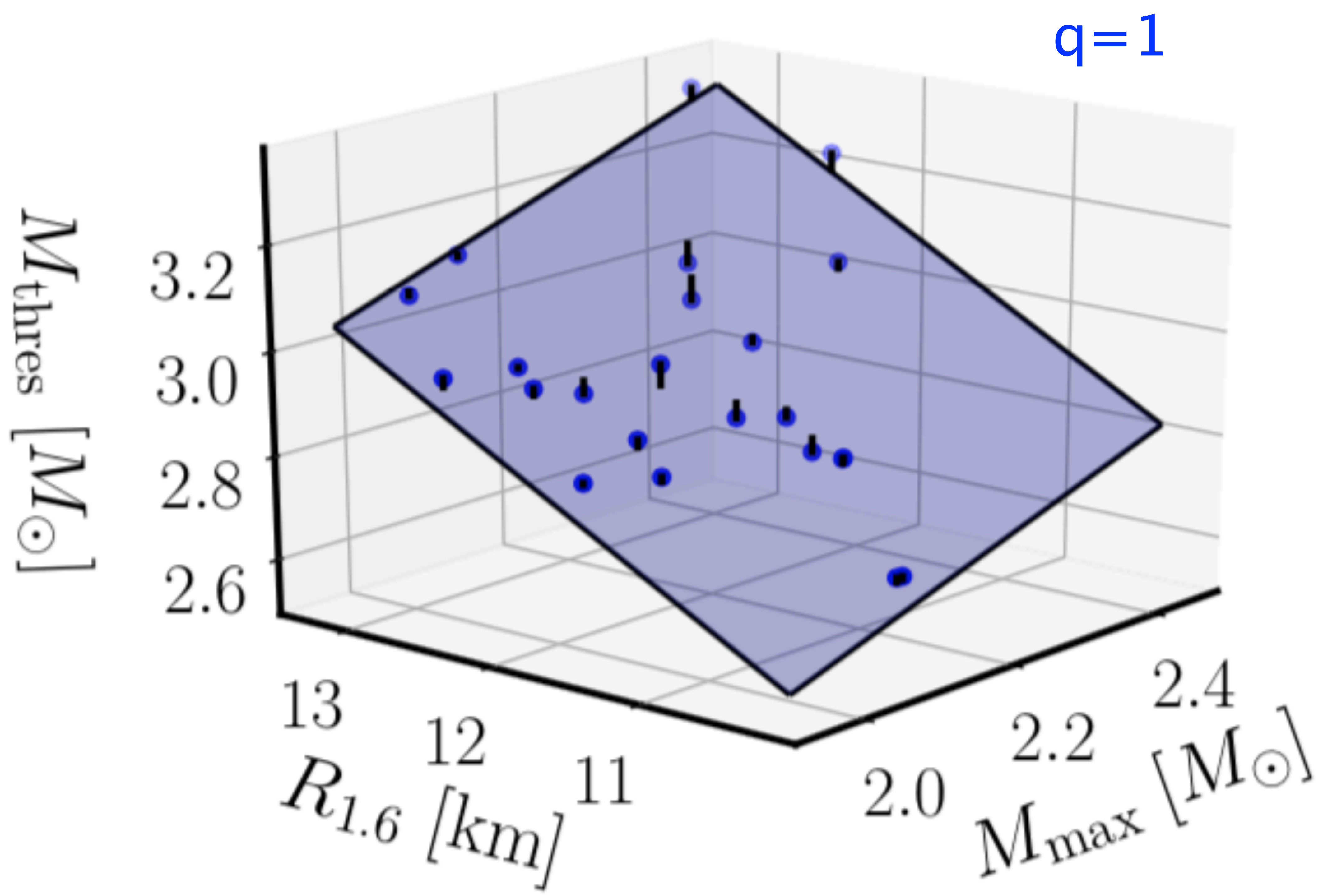

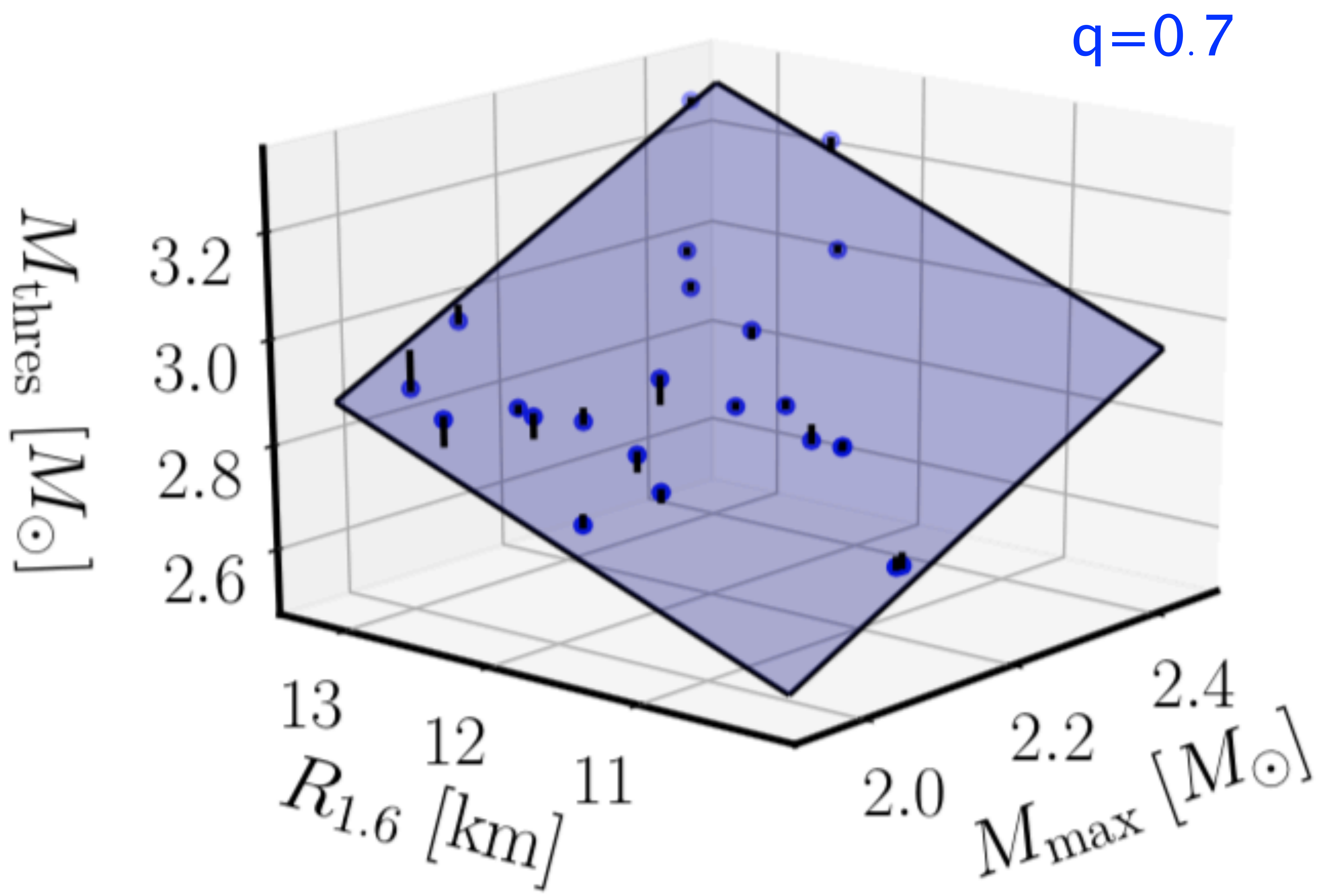

$$M_{\rm thres}(M_\odot) = 0.547 M_{\rm max} + 0.165 R_{1.6} - 0.198 \quad (\pm 0.042)$$

(max. dev.)

$$M_{\rm thres}(M_\odot) = 0.832 M_{\rm max} + 0.116 R_{1.6} - 0.276 \quad (\pm 0.067)$$

(max. dev.)

q–DEPENDENT EMPIRICAL RELATION FOR SPECIFIC EOS

For a few EOS we construct a fit in the range $0.5 \leq q \leq 1$ of the form

$$\boxed{M_{\rm thres}\ (q) = \alpha(1-q)^n + \gamma}$$

and find that $2.5 \leq n \leq 3.5$ within this sample.

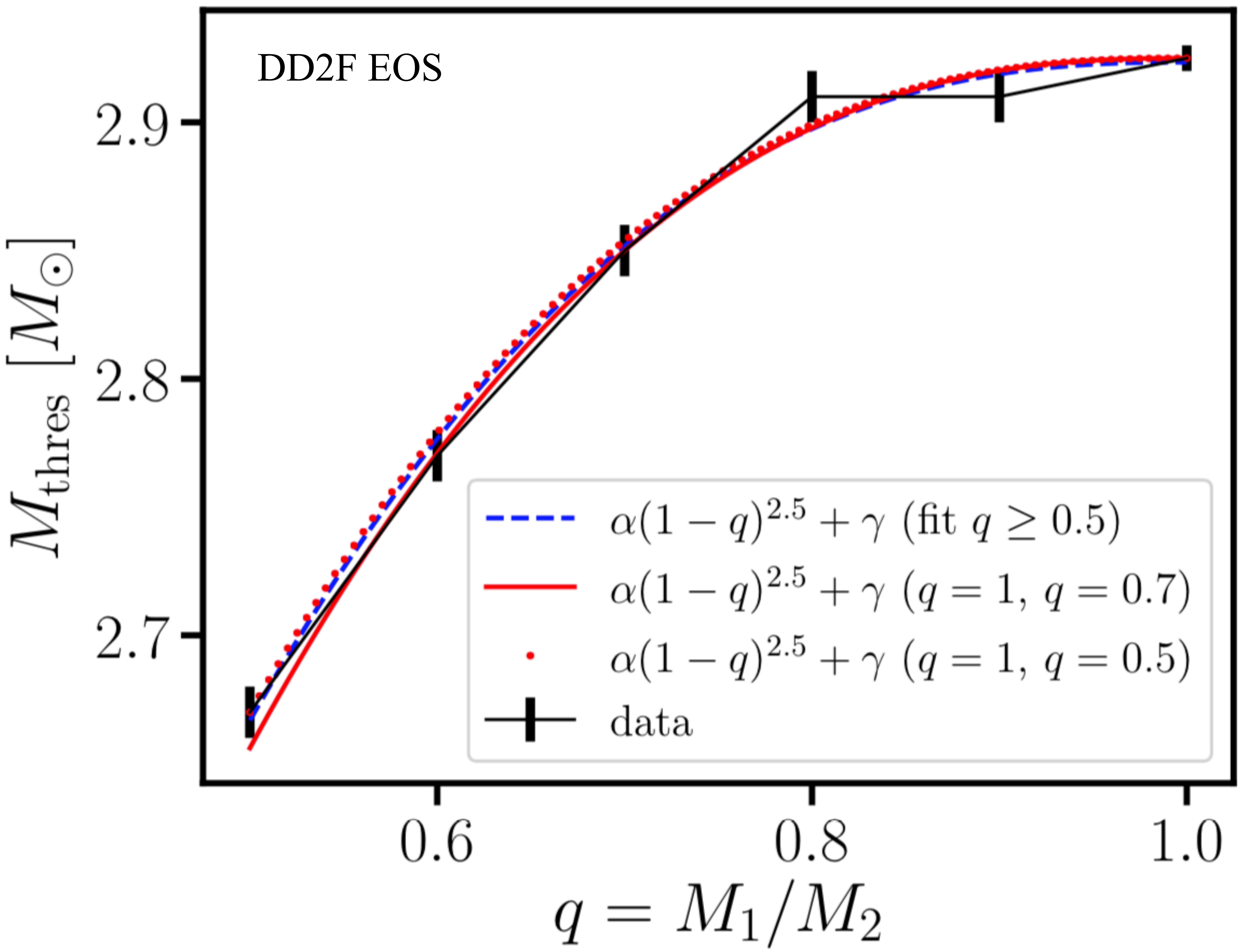

GENERALIZED EMPIRICAL RELATION FOR THRESHOLD MASS

We take n=3 as an average value and arrive at the **generalized empirical** relation that also depends on the mass ratio:

$$M_{\rm thres}\ (q, M_{\rm max}, R_{1.6}) = c_1 M_{\rm max} + c_2 R_{1.6} + c_3 + c_4 \delta q^3 M_{\rm max} + c_5 \delta q^3 R_{1.6} + c_6 \delta q^3$$

$$\delta q \equiv 1 - q$$

For the base sample q=1 and q=0.7 with 23 hadronic EOS, the maximum residual is only $0.067 M_\odot$.

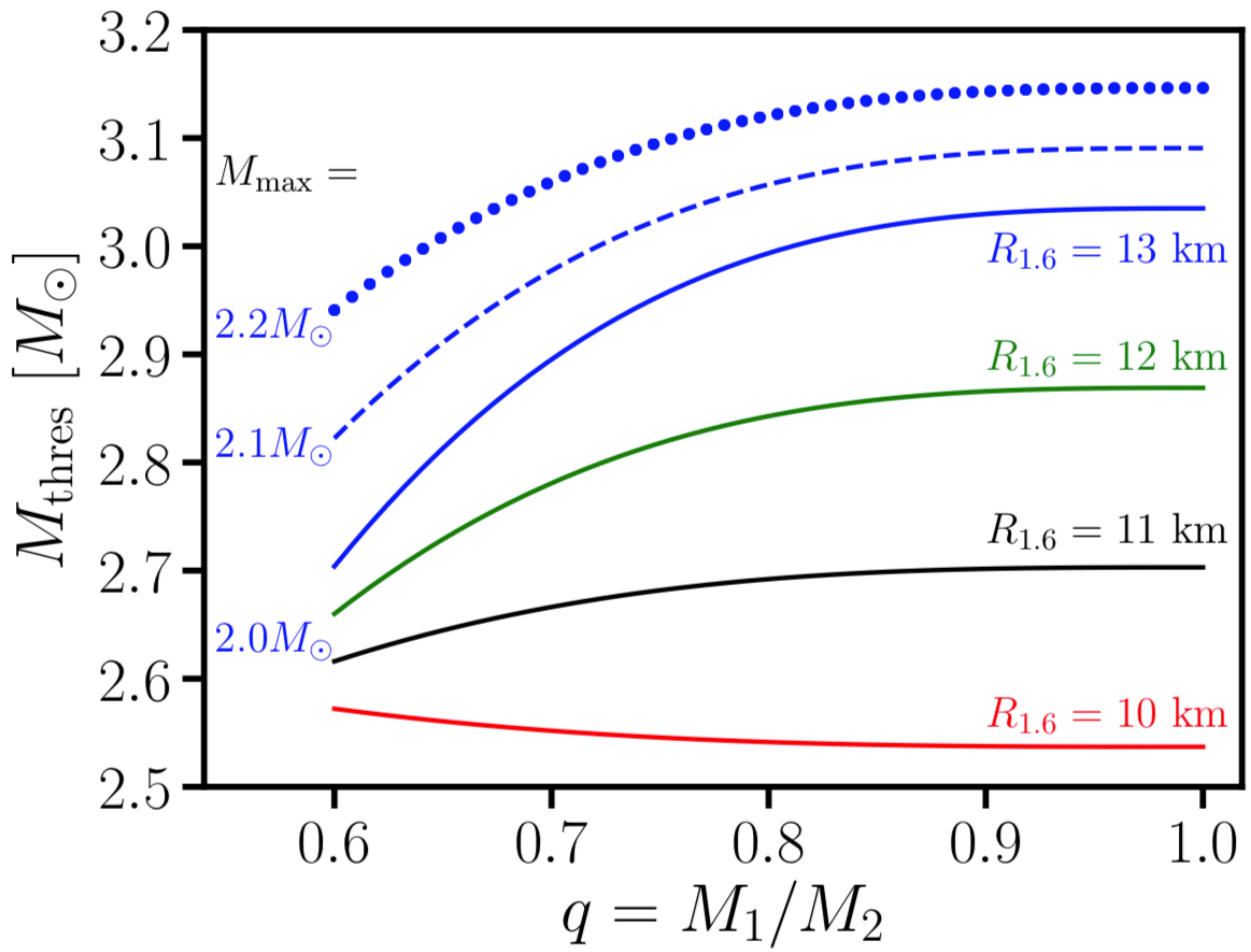

ROTATION PROFILE OF BNS REMNANTS

Key properties:

- Maximum angular velocity about twice the central angular velocity

$$\Omega_{\mathrm{max}} \sim 2\Omega_c$$

- Angular velocity at equator comparable to central angular velocity

$$\Omega_{\mathrm{e}} \sim \Omega_c$$

- Central angular velocity mostly due to frame dragging

$$\Omega \sim \omega$$

- Frequency of main post-merger GW peak about half of the maximum angular velocity

$$\Omega_{\mathrm{max}} \sim \Omega_{\mathrm{GW}}/2$$

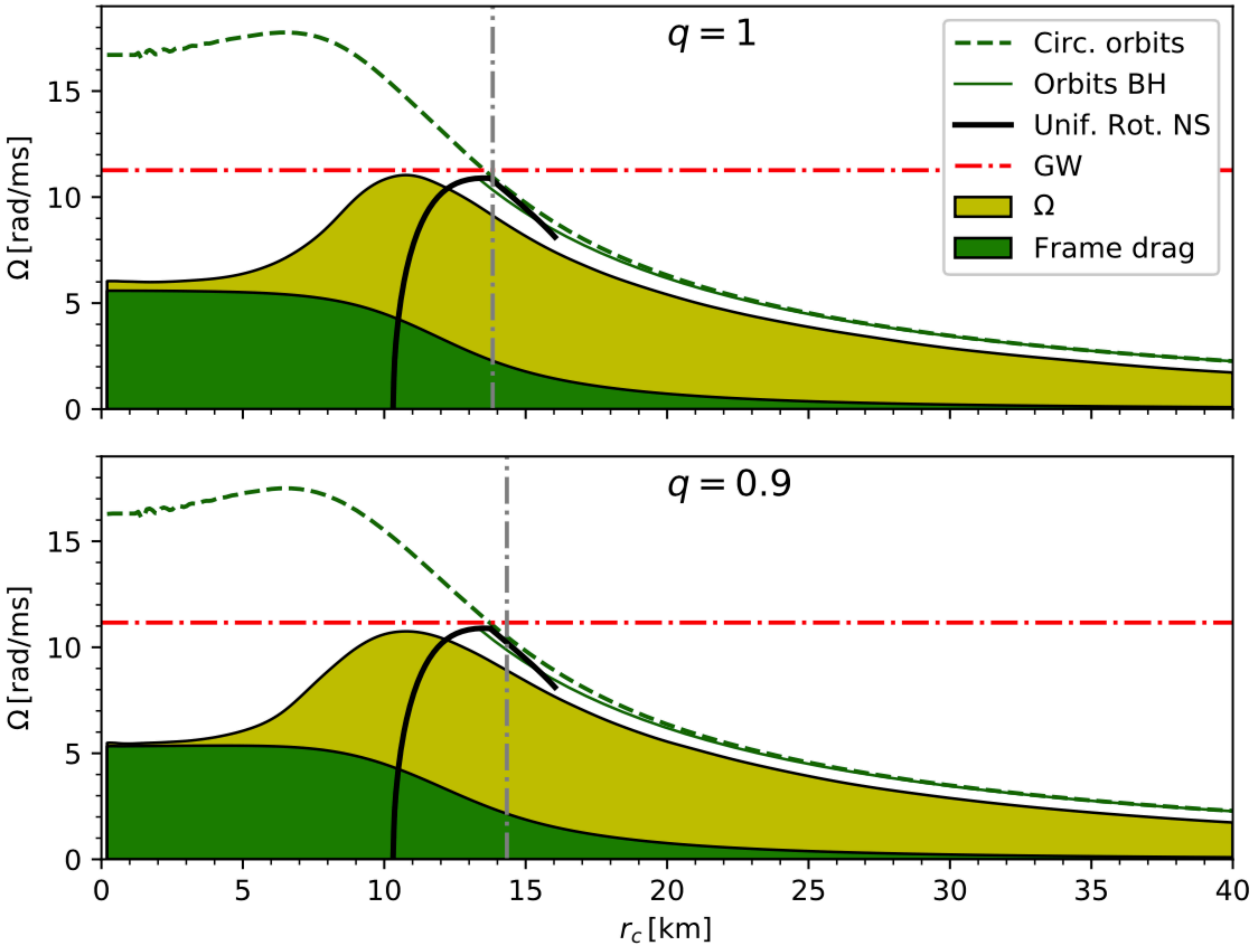

Kastaun, Galeazzi (2015); Kastaun, Ohme (2021)

Cold core + hot envelope of several tens MeV.

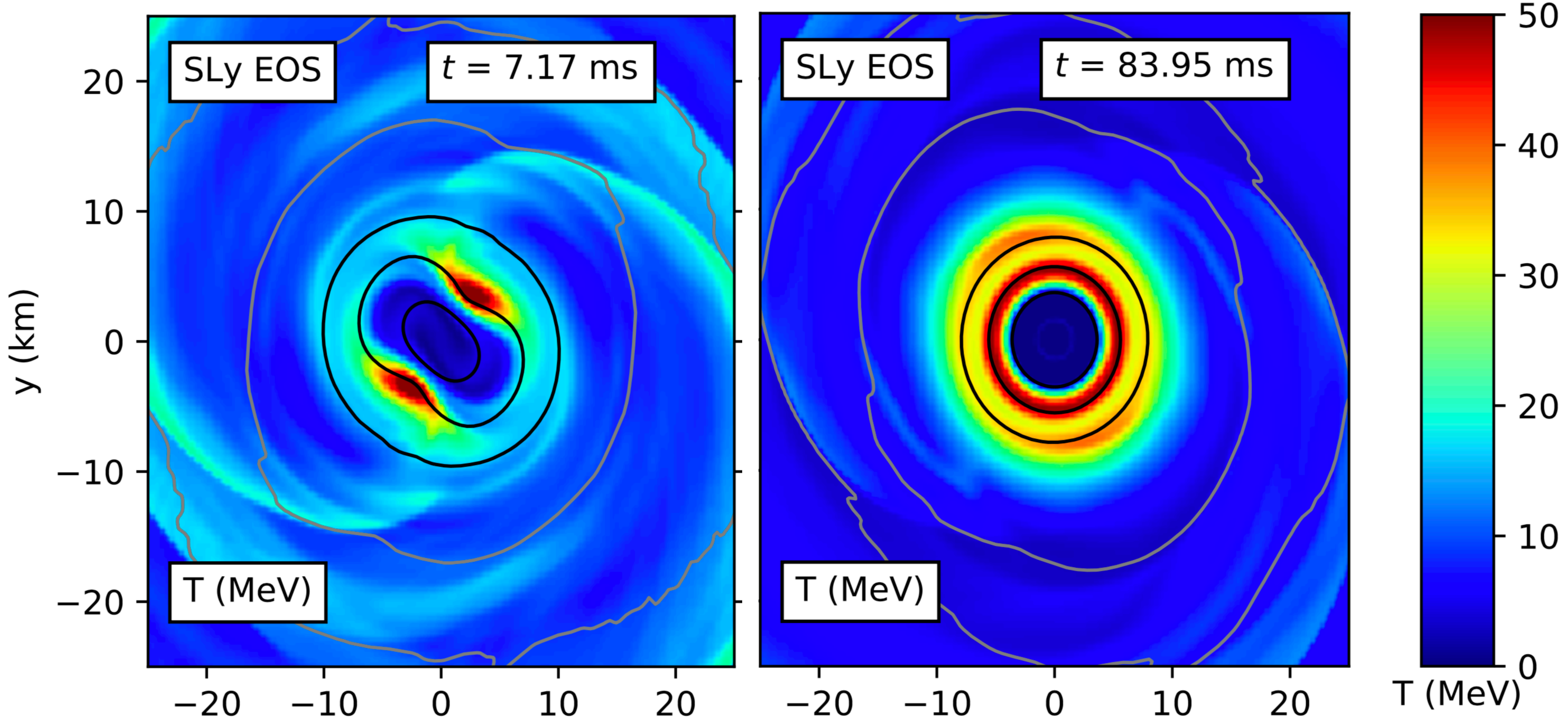

De Pietri et al. (2019)

ANGULAR MOMENTUM OF POST-MERGER REMNANTS

The angular momentum of post-merger remnants at the moment of collapse is given by an EOS-insensitive empirical relation of the form (Bauswein, Stergioulas, 2017)

$$\frac{cJ_{\rm merger}}{GM_\odot^2} \simeq a\frac{M_{\rm tot}}{M_\odot} - \left(b + \frac{R_{1.5} - R_{1.5}^{\rm DD2}}{10\ {\rm km}}\right)$$

with a=4.041 and b=4.658.

An alternative form is (Lucca et al. 2021)

$$\frac{GJ_{\rm merger}}{c^3 R_{\rm NS}^2} = 0.875 C_{\rm NS} - 5.209$$

Where $C_{\rm NS} = GM_{\rm NS}/c^2 R_{\rm NS}$ is the compactness of a TOV model with $M_{\rm NS} = M_{\rm tot}/2$

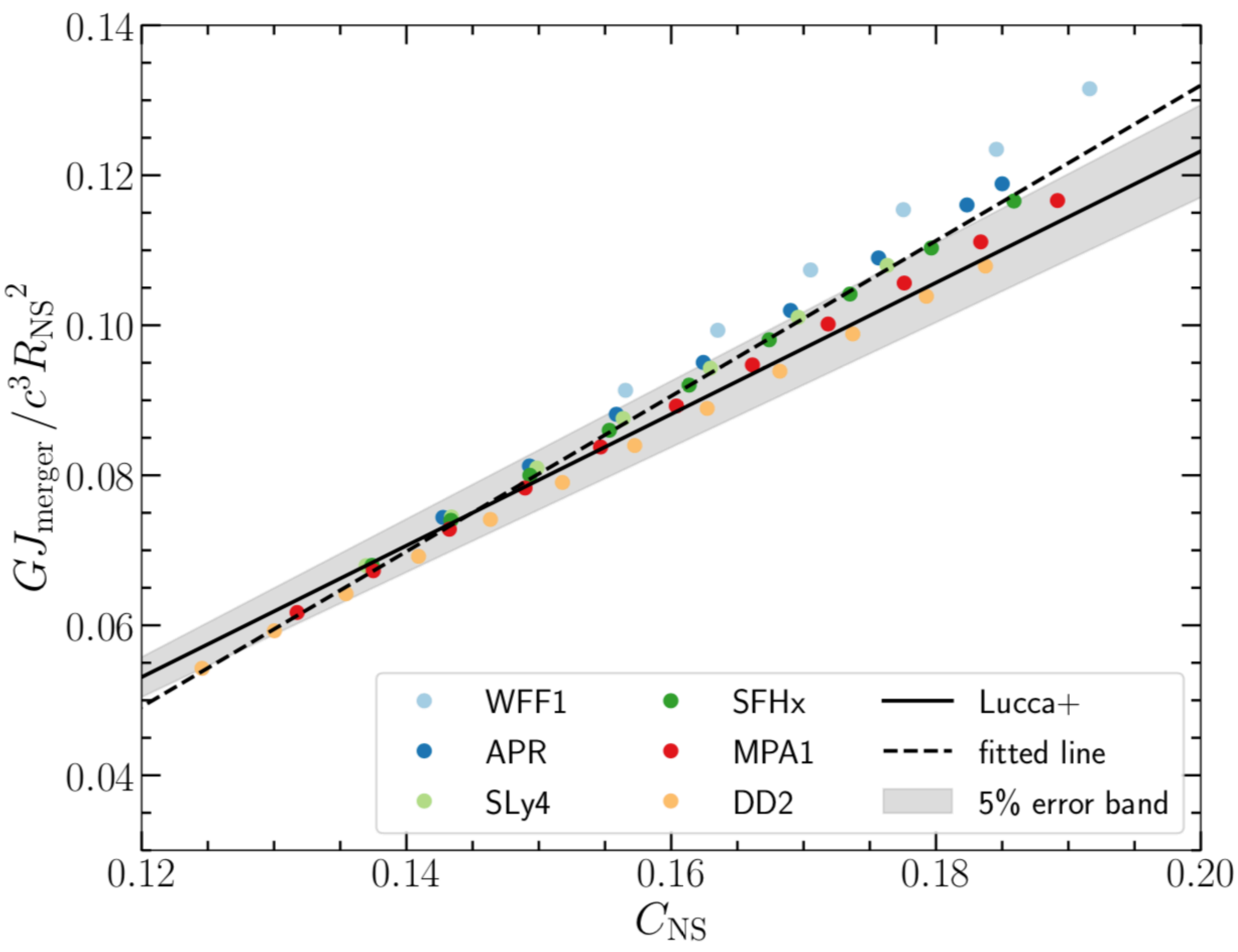

Iosif, Stergioulas (2021)

EQUILIBRIUM MODELS OF POST-MERGER REMNANTS

We construct merger sequences of equilibrium models of post-merger remnants, with the following characteristics:

- 4-parameter rotation law by Uryu et al. (2017), with p=1, q=3.

$$\Omega = \Omega_c \frac{1 + \left(\frac{F}{B^2 \Omega_c}\right)^p}{1 + \left(\frac{F}{A^2 \Omega_c}\right)^{q+p}} \qquad F \equiv u^t u_\phi$$

- The remaining two parameters A, B are redefined as

$$\lambda_1 \equiv \frac{\Omega_{\rm max}}{\Omega_c} \qquad \lambda_2 \equiv \frac{\Omega_e}{\Omega_c}$$

- We consider 3 hadronic EOS with radii between 11km and 13km for typical NS.

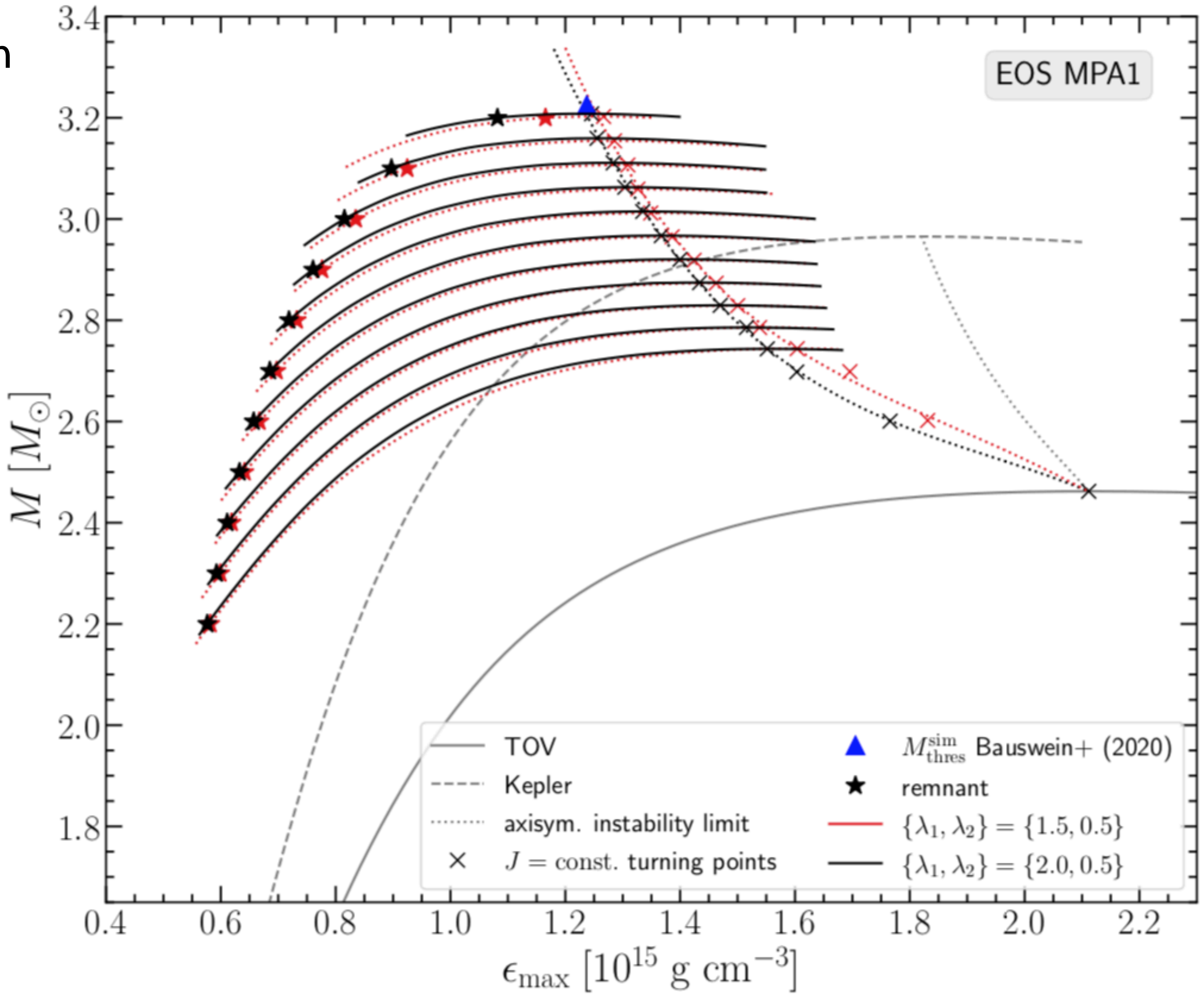

REPRODUCTION OF THE THRESHOLD MASS

The intersection between the sequence of merger remnants and the turning-point line determines a threshold mass that agrees remarkably well for all 3 EOS.

EOS $\{\lambda_1, \lambda_2\}$	$M^{\rm eq}_{\rm thres}$ $[M_\odot]$	$J^{\rm eq}_{\rm thres}$ $[\frac{GM^2_\odot}{c}]$	$M^{\rm sim}_{\rm thres}$ $[M_\odot]$	$\delta M_{\rm thres}$ [%]
APR			2.825	
{2.0, 0.5}	2.851	6.524		0.92
{1.5, 0.5}	2.842	6.492		0.60
DD2			3.325	
{2.0, 0.5}	3.302	8.766		0.69
{1.5, 0.5}	3.285	8.697		1.20
MPA1			3.225	
{2.0, 0.5}	3.201	8.136		0.74
{1.5, 0.5}	3.192	8.100		1.02

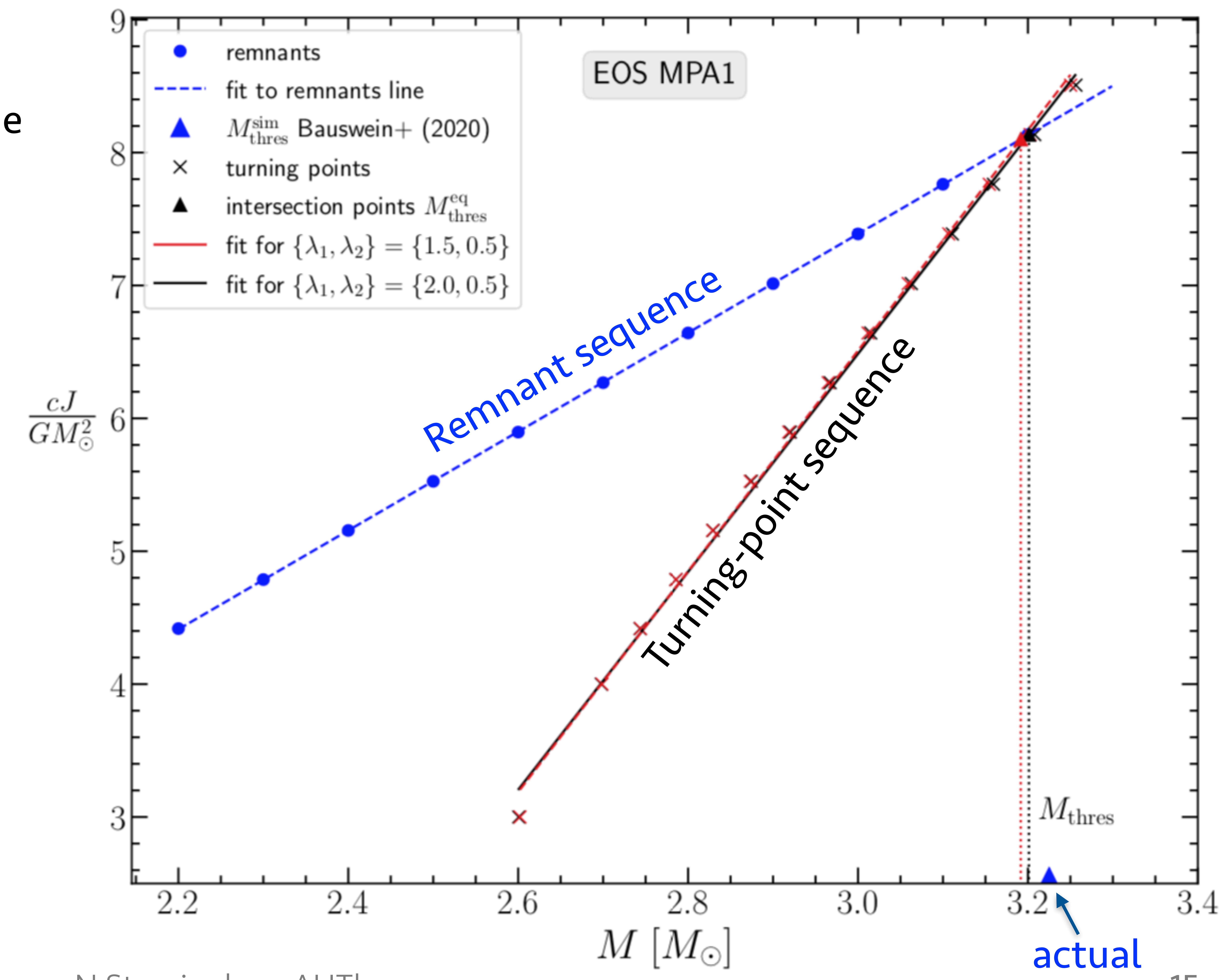

ROTATION PROFILES

The rotation profiles show a qualitative agreement with those extracted from simulations.

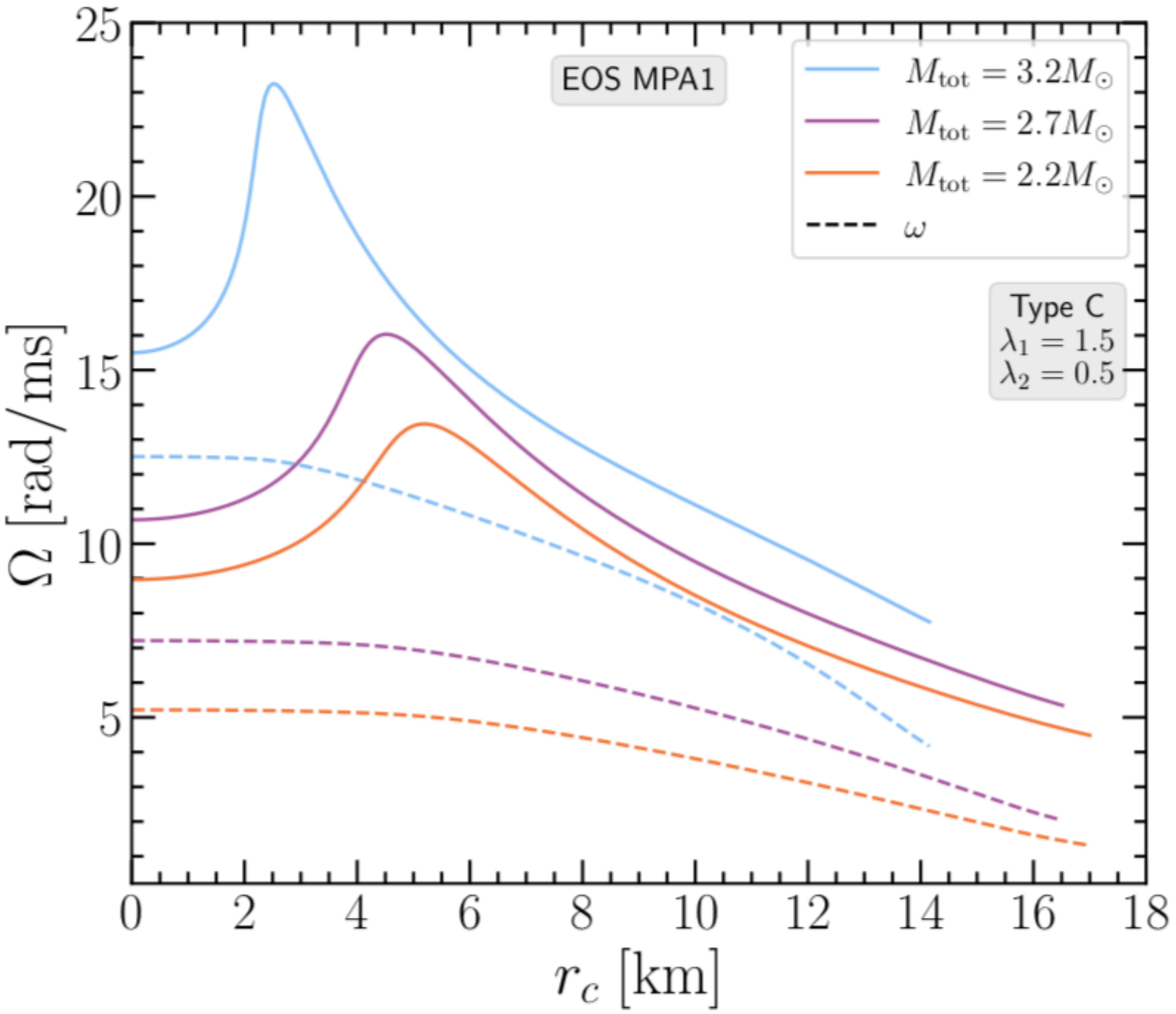

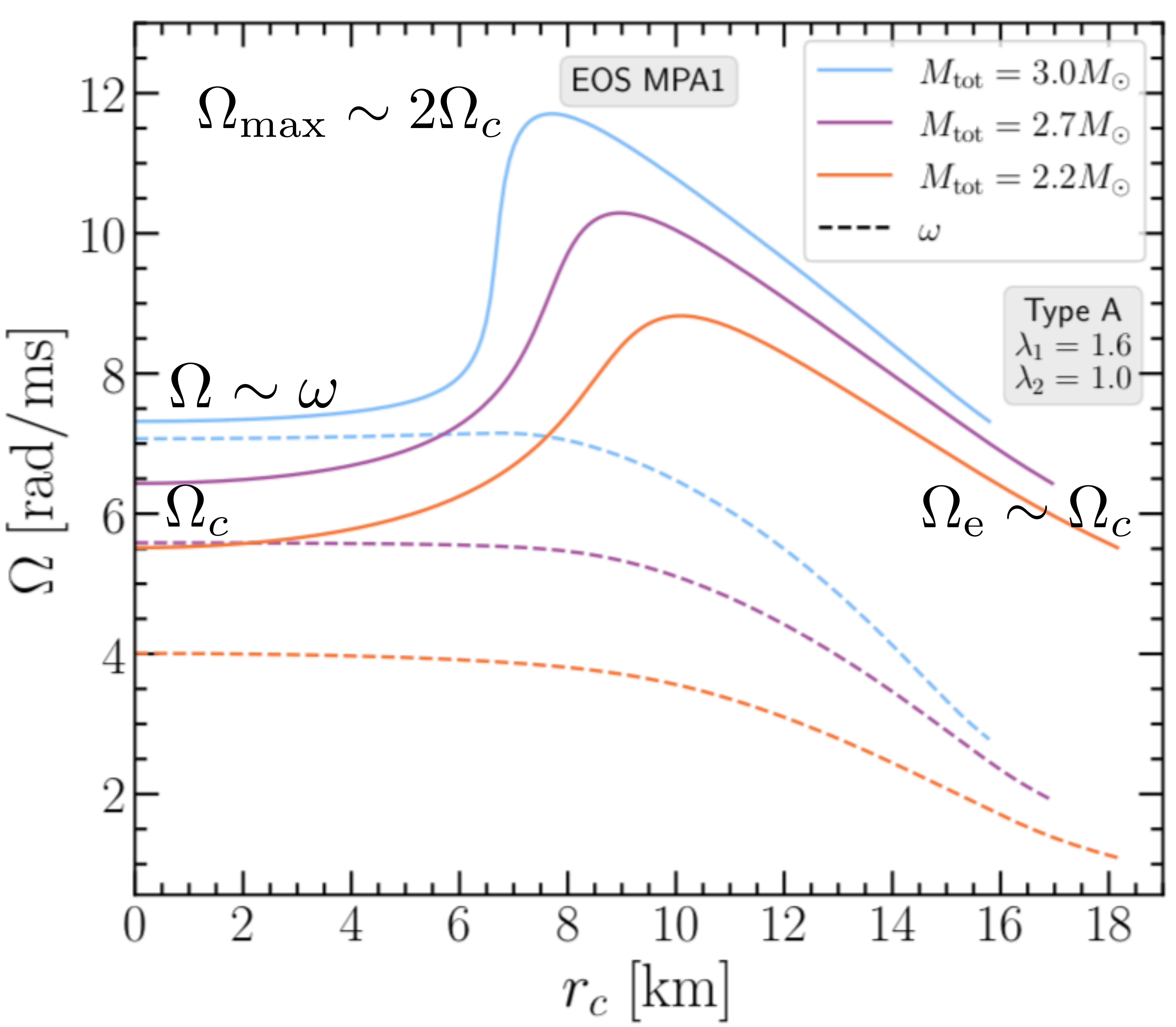

DENSITY DISTRIBUTION OF REMNANT MODELS

We find both quasi-toroidal (Type C) and quasi-spherical (Type A) models.

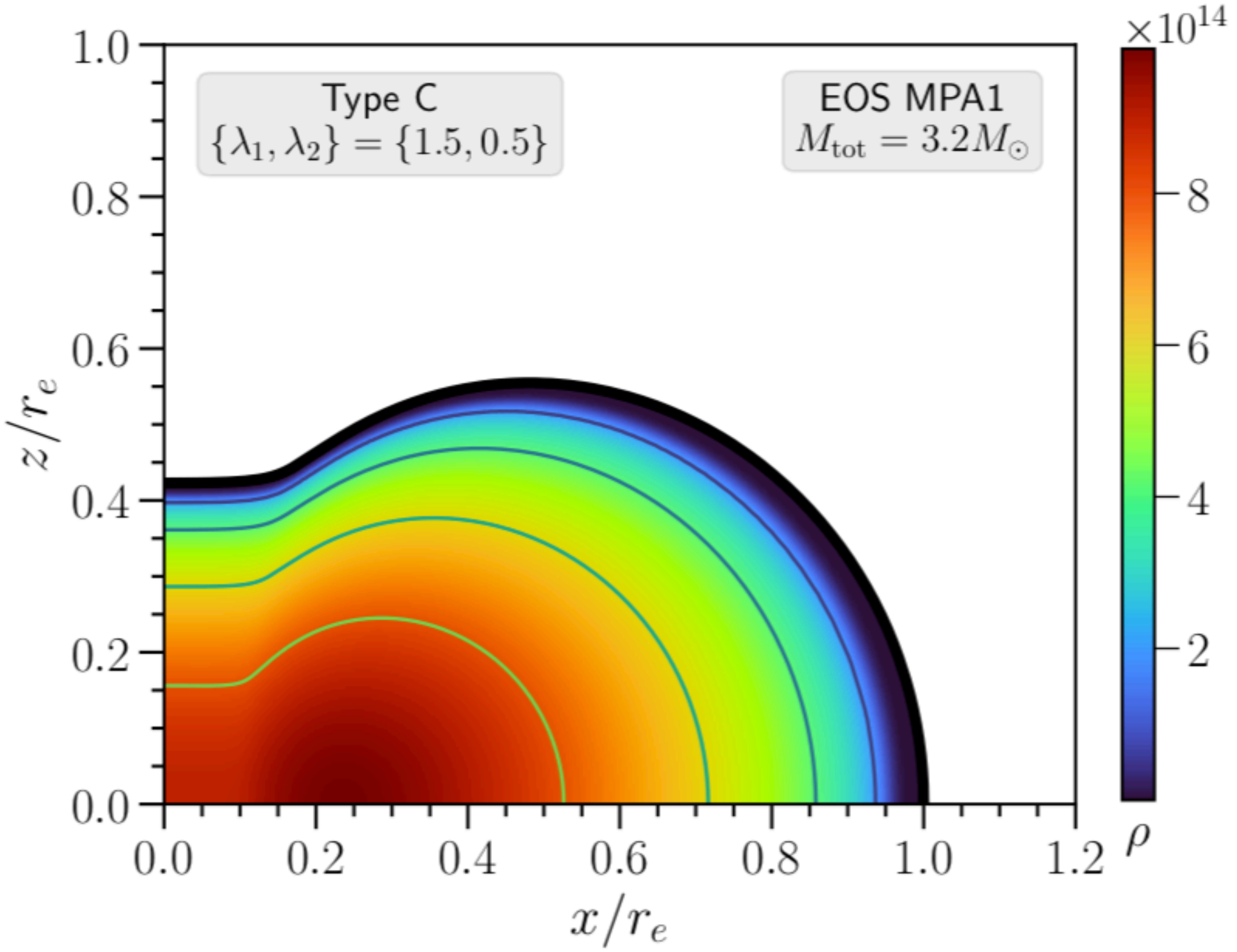

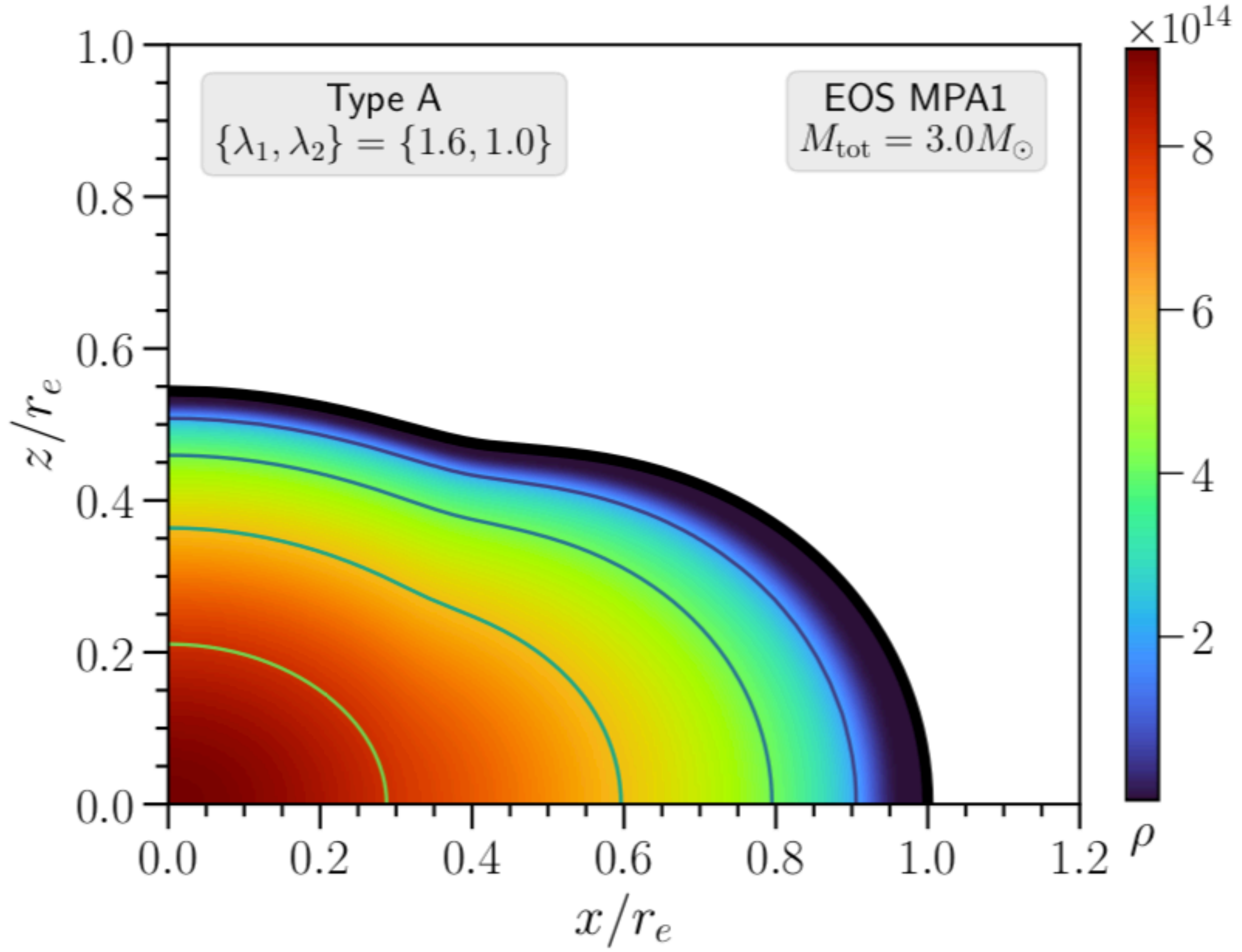

We define the "equatorial compactness" as

$$C_e = M/R_e$$

and find that the models at the threshold mass have

$$C_e \sim 0.33$$

This supports the conjecture by Kastaun, Ohme (2021) that remnants collapse when their slowly rotating, cold core has a compactness comparable to $C_{\max}^{\mathrm{TOV}}$.

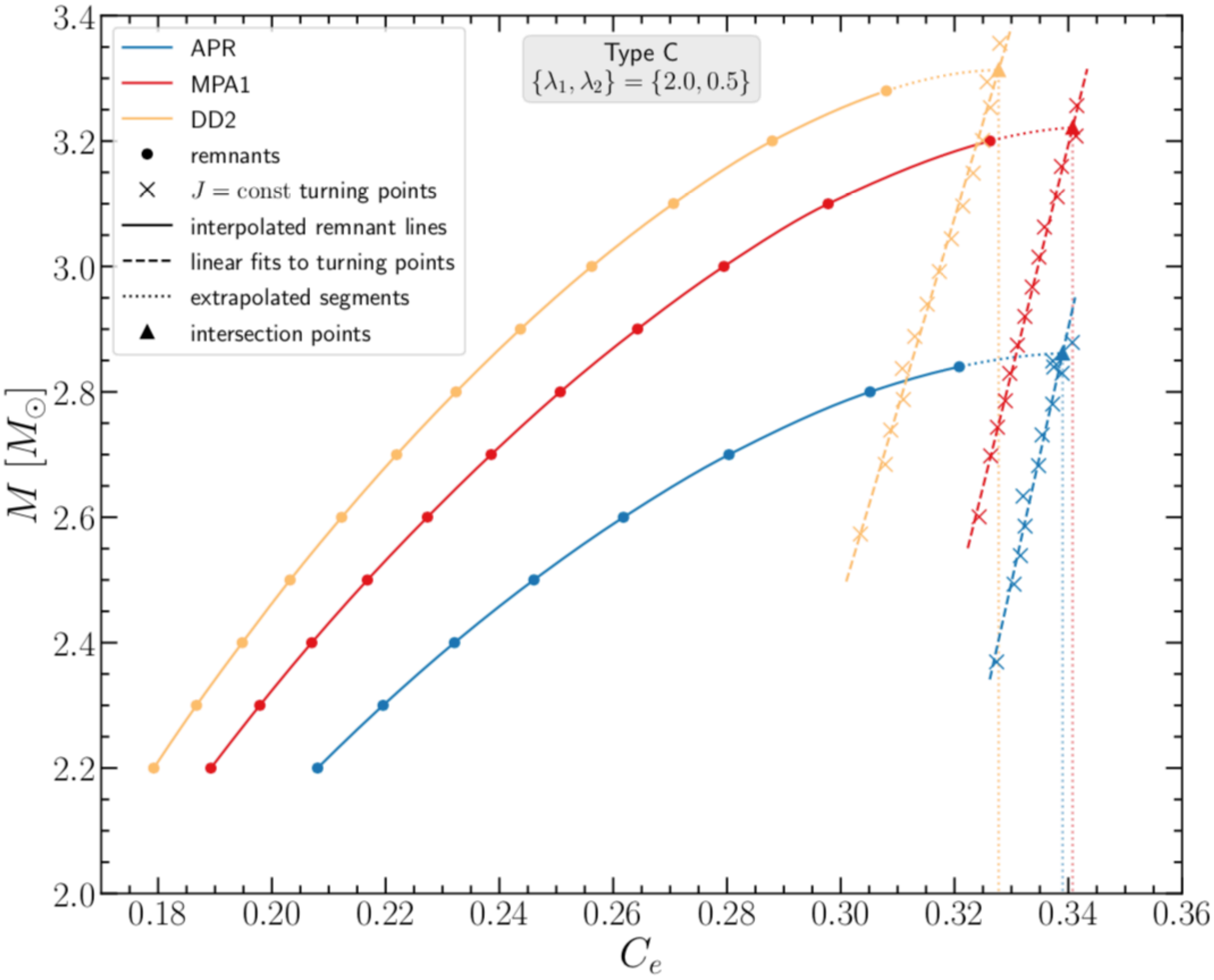

The GW signal can be divided into three distinct phases:
inspiral, *merger* and *post-merger oscillations*.

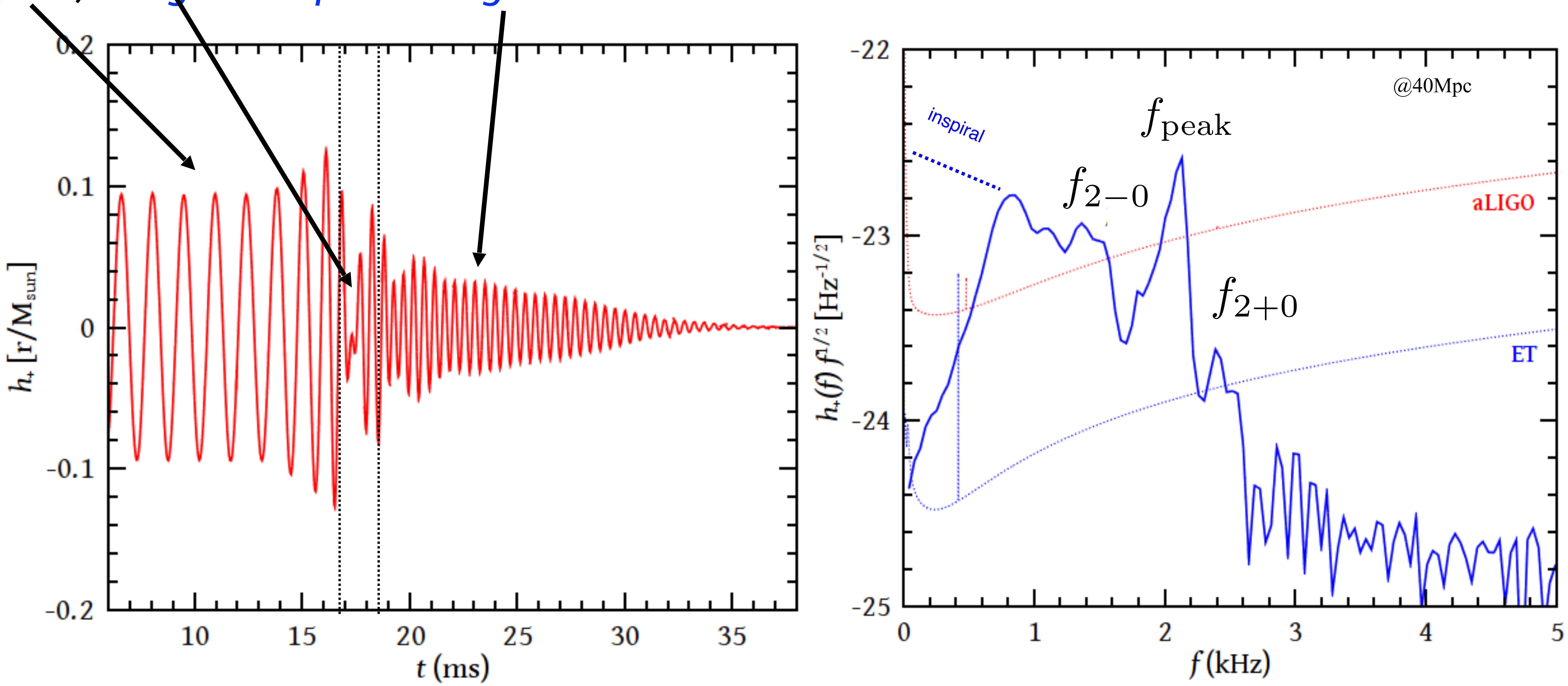

$$f_{\rm peak} = f_2$$

is due to the fundamental $l=m=2$ f-mode oscillation

$$f_{2-0} = f_2 - f_0$$
$$f_{2+0} = f_2 + f_0$$

are quasi-linear combination tones

Stergioulas et al. (2011)

Orbiting spiral arms also lead to a distinct frequency

$$f_{\mathrm{spiral}}$$

Bauswein & Stergioulas (2015)

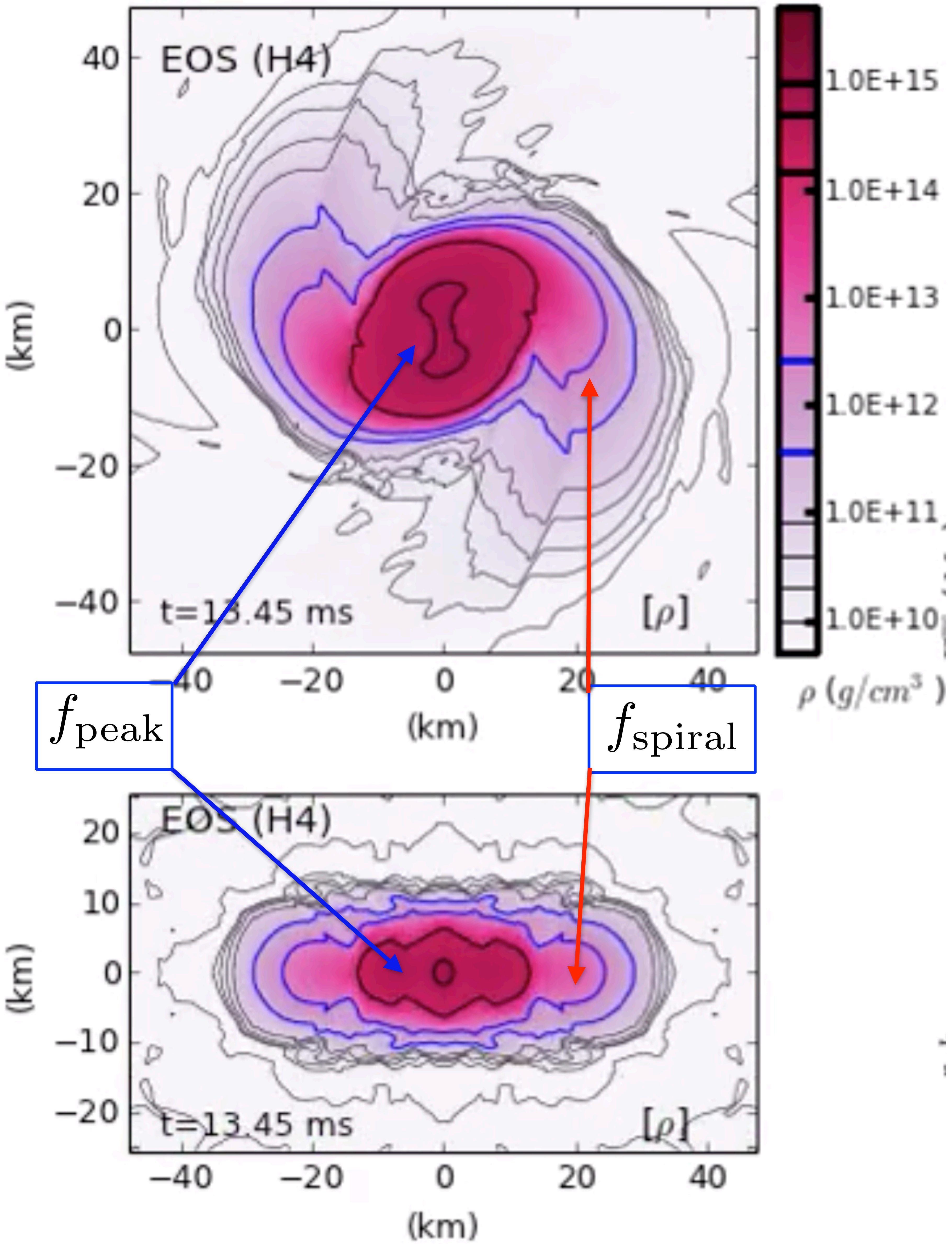

SPECTRAL CLASSIFICATION OF POST-MERGER GW EMISSION

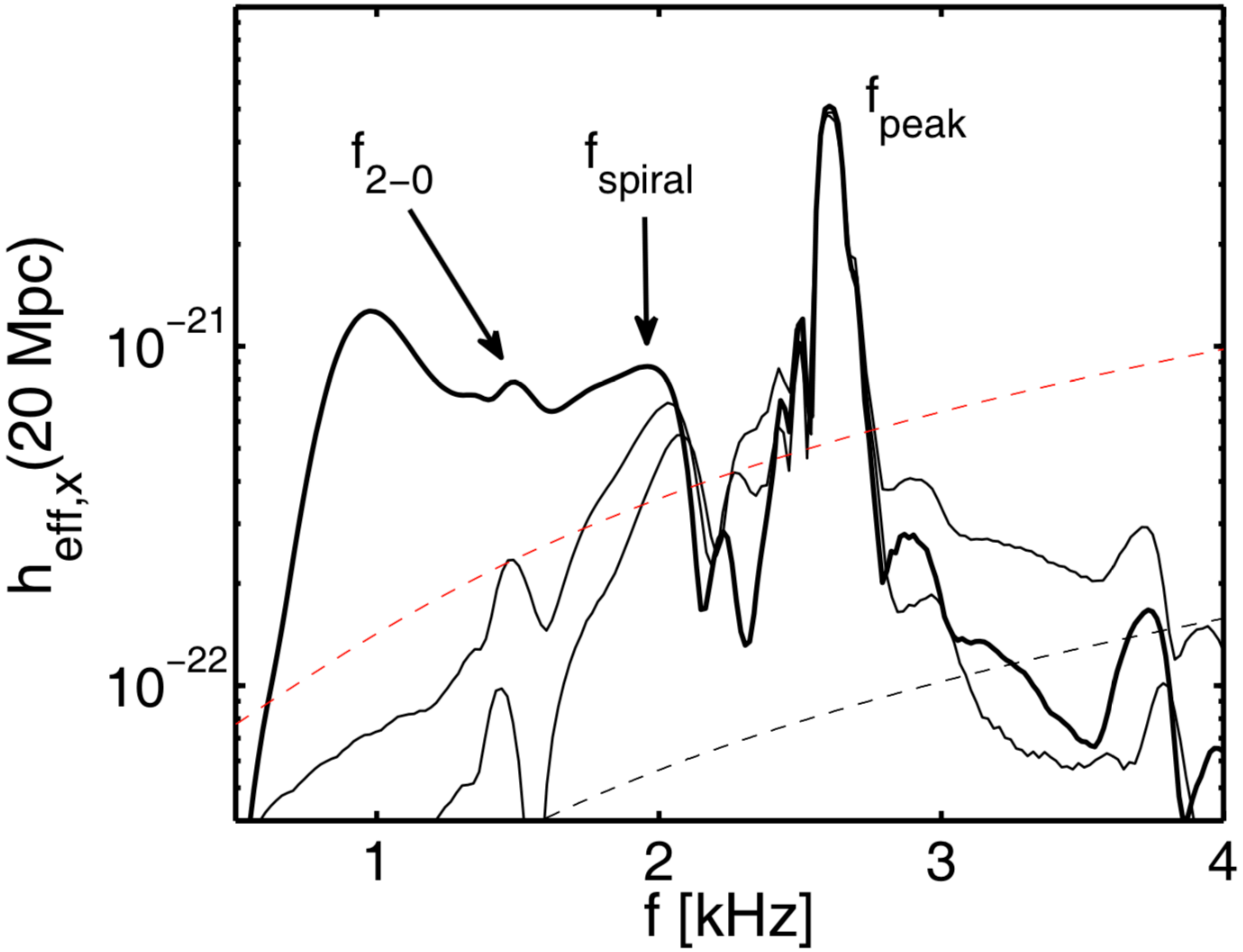

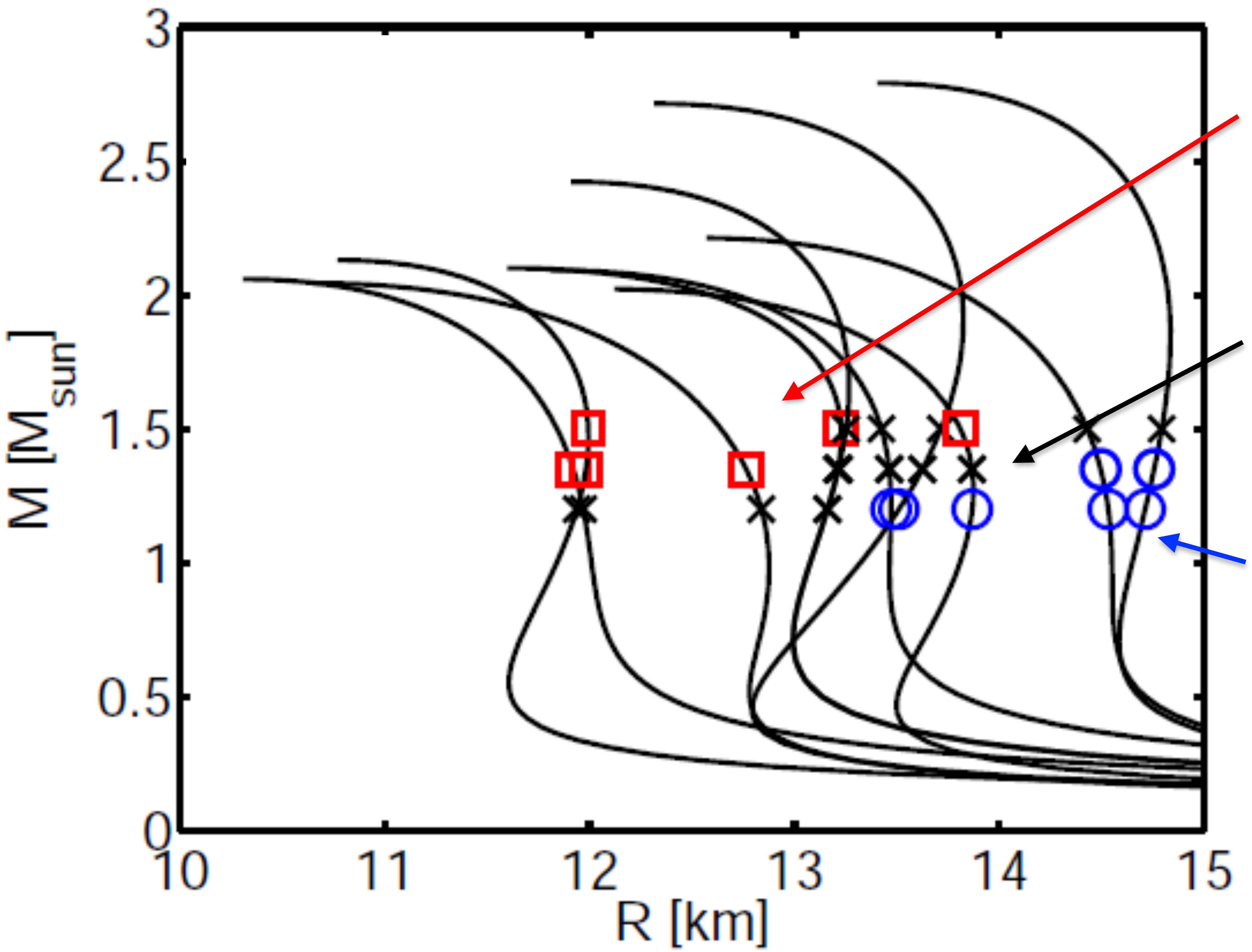

Type I:

$A_{2-0} > A_{\rm spiral}$

Type II:

$A_{2-0} \sim A_{\rm spiral}$

Type III:

$A_{2-0} < A_{\rm spiral}$

Bauswein & Stergioulas (2015)

RADIUS DETERMINATION THROUGH POST-MERGER GWs

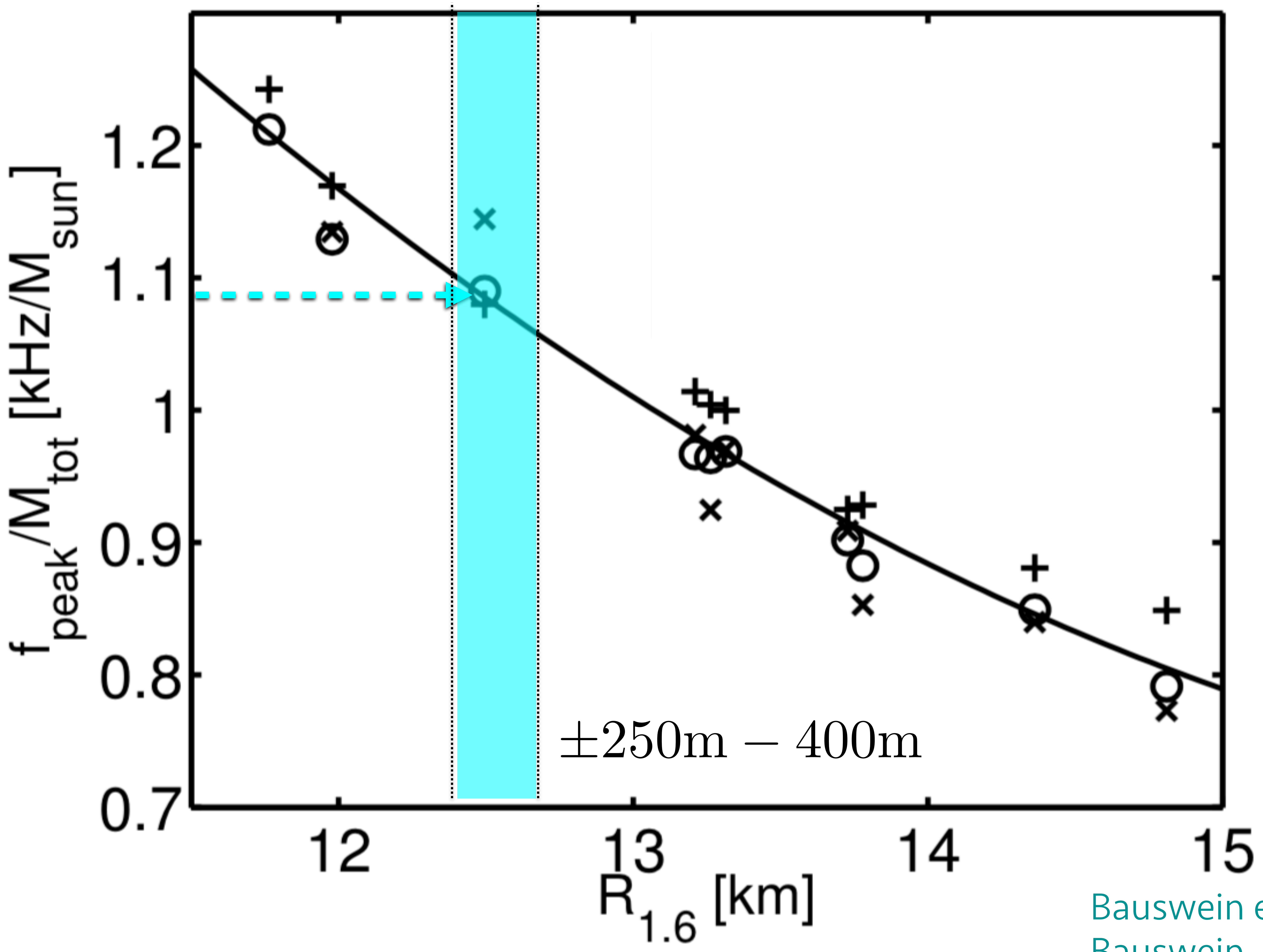

Bauswein et al. (2012)
Bauswein, Stergioulas, Janka (2016)

EMPIRICAL RELATIONS FOR GW ASTEROSEISMOLOGY OF BNS MERGERS

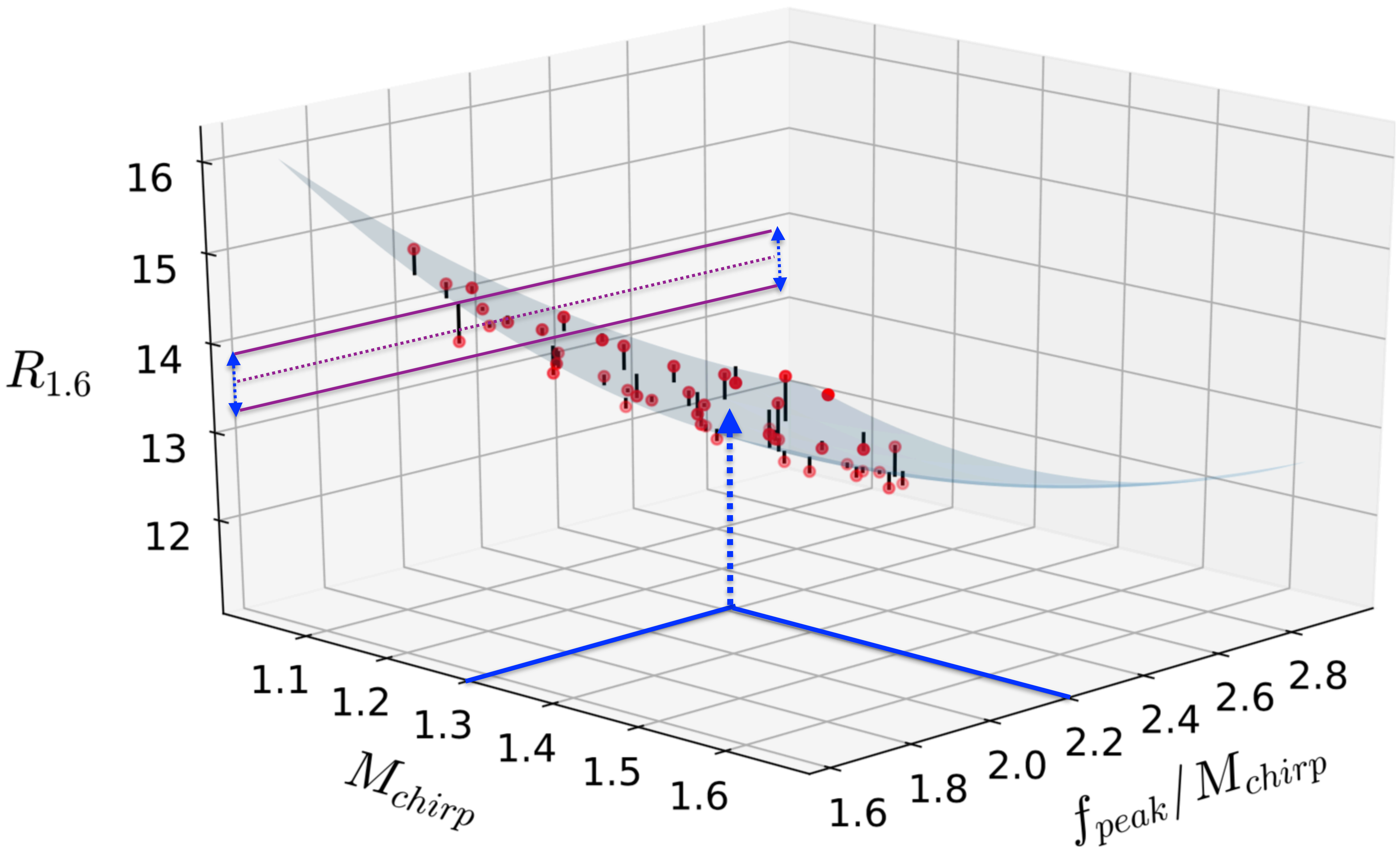

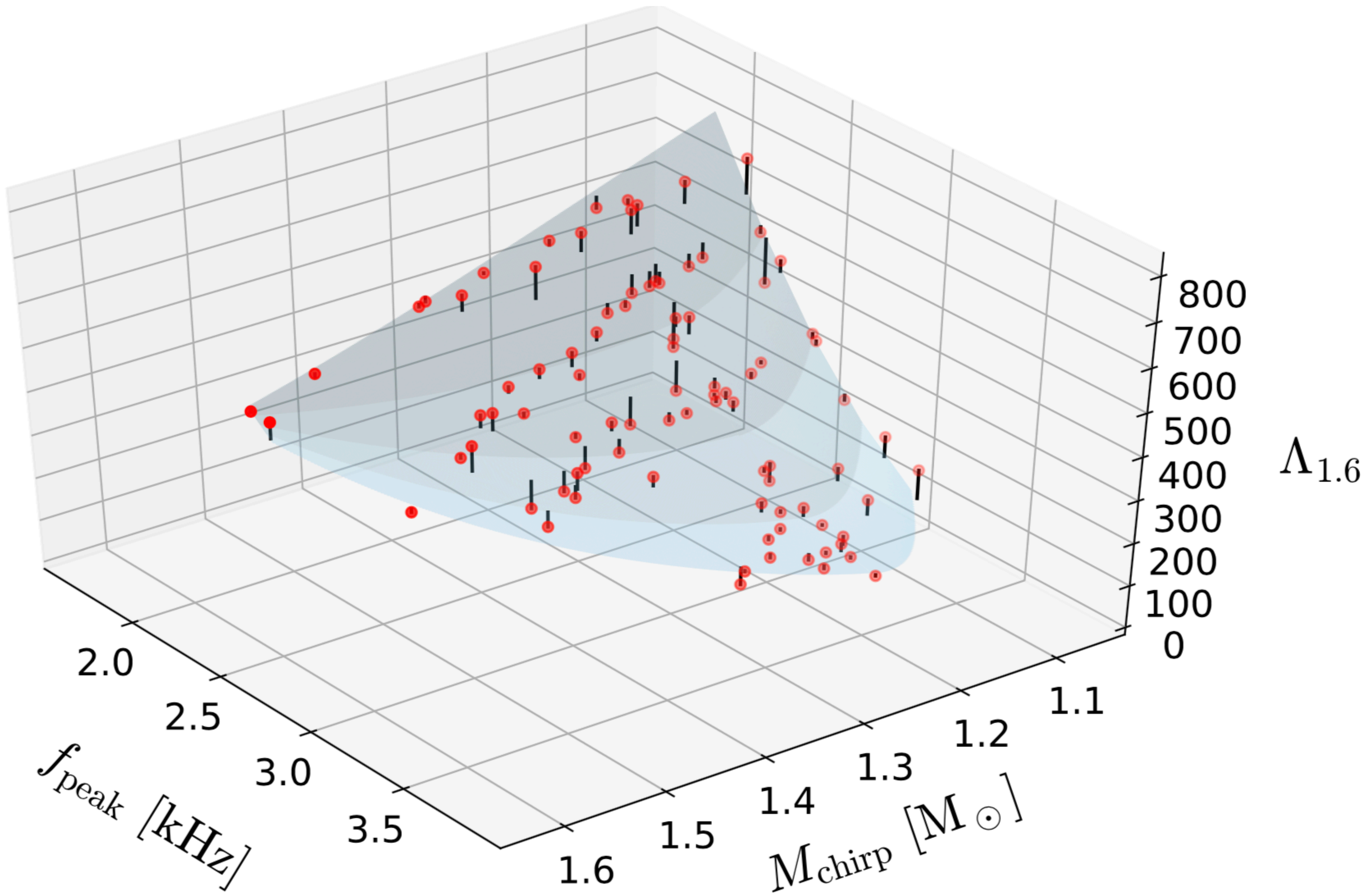

Vretinaris, Stergioulas & Bauswein (2020) l=2 mode in nonrotating NS

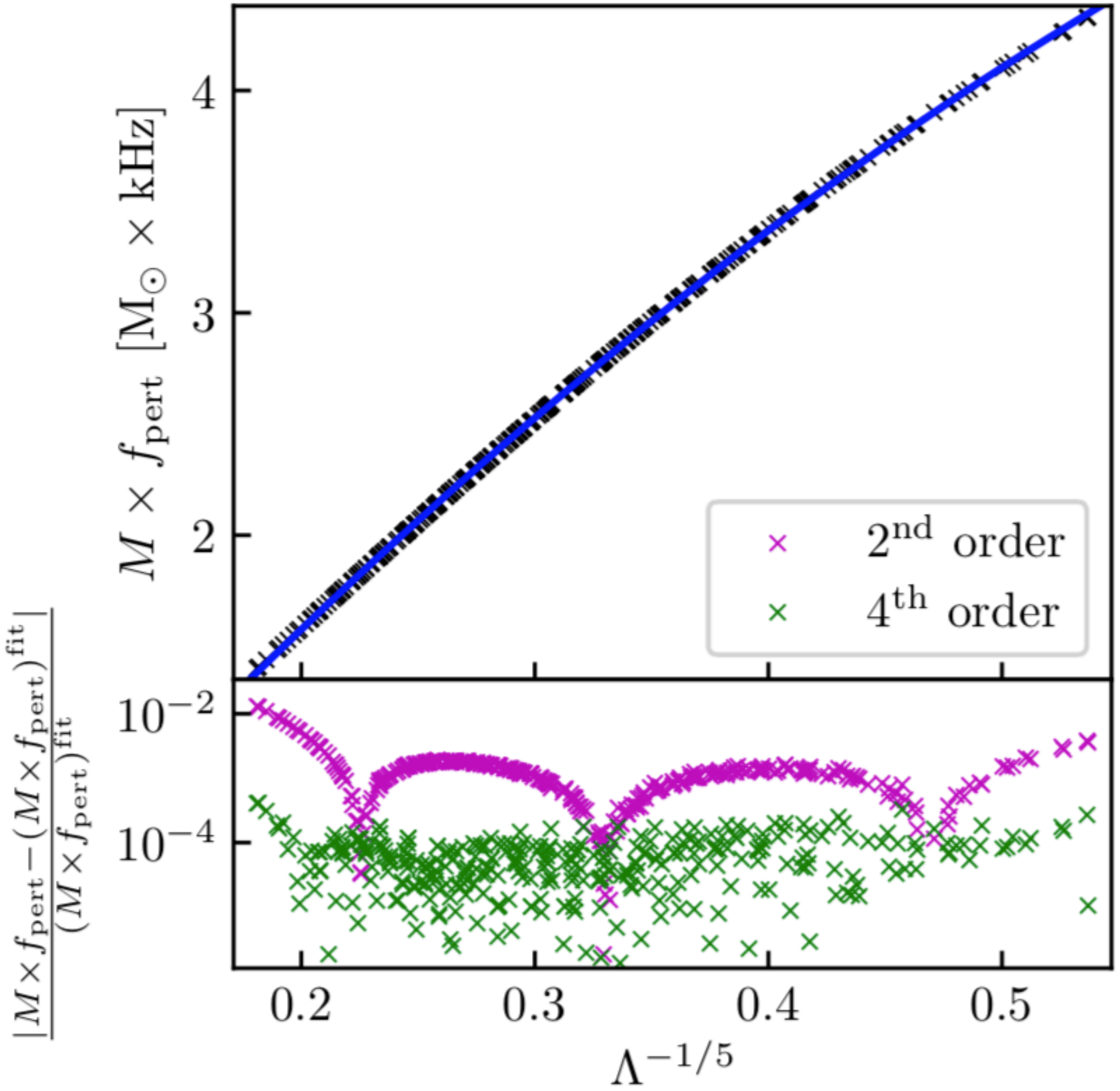

Lioutas, Bauswein, Stergioulas (2021)

$$M f_{\rm pert} = -0.24 + 7.726\Lambda^{-1/5} + 11.88\Lambda^{-2/5} - 27.65\Lambda^{-3/5} + 15.39\Lambda^{-4/5}$$

NEW UNIVERSAL RELATIONS BETWEEN REMNANTS AND NONROTATING STARS

- Using the correspondence $M_{\rm TOV} = \sqrt[5]{2} \times M_{\rm tot}/2$

f_{peak} (post-merger) vs. f_{pert} (nonrotating star)

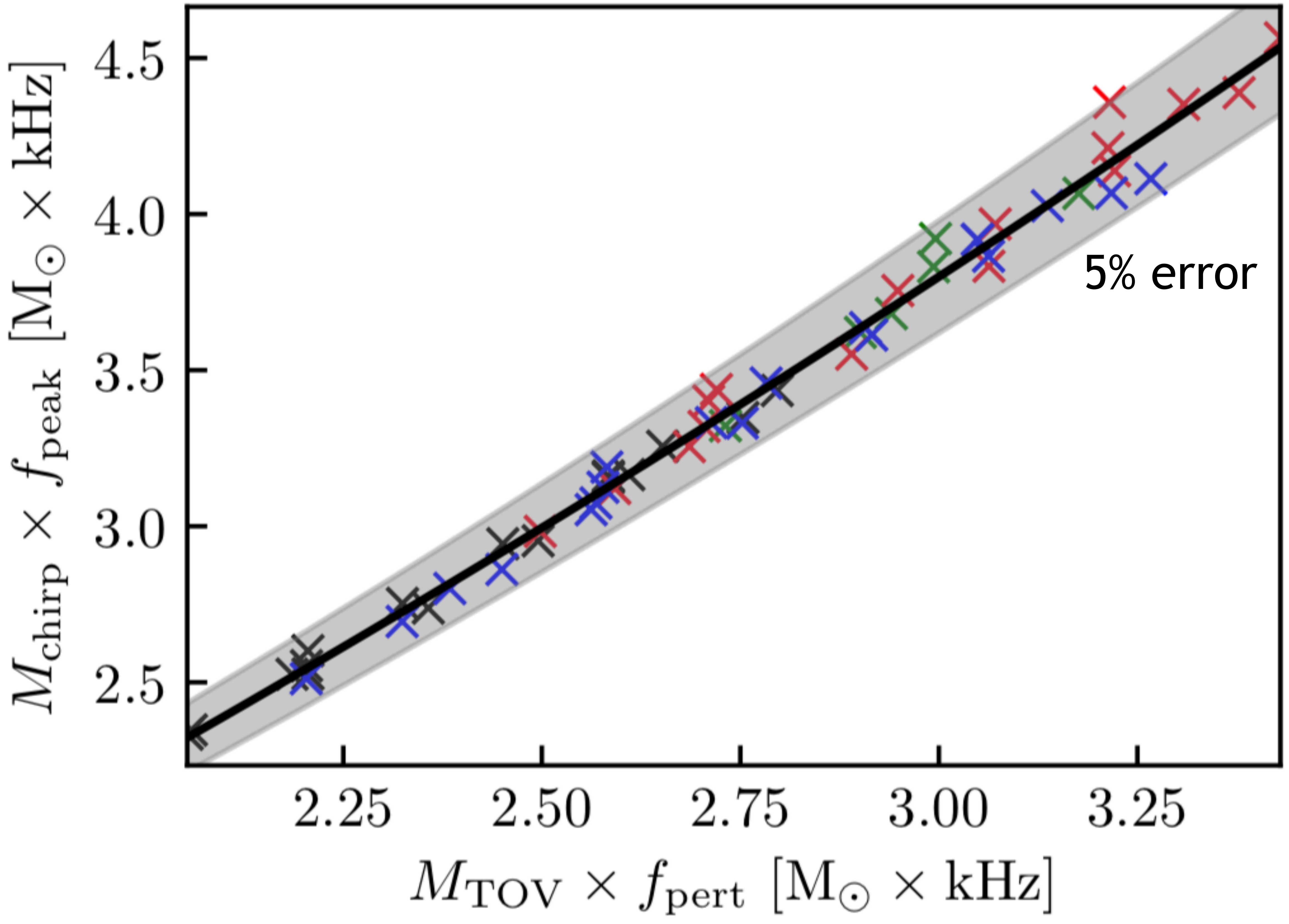

f_{peak} (post-merger) vs. $\Lambda^{1/5}$ (nonrotating star)

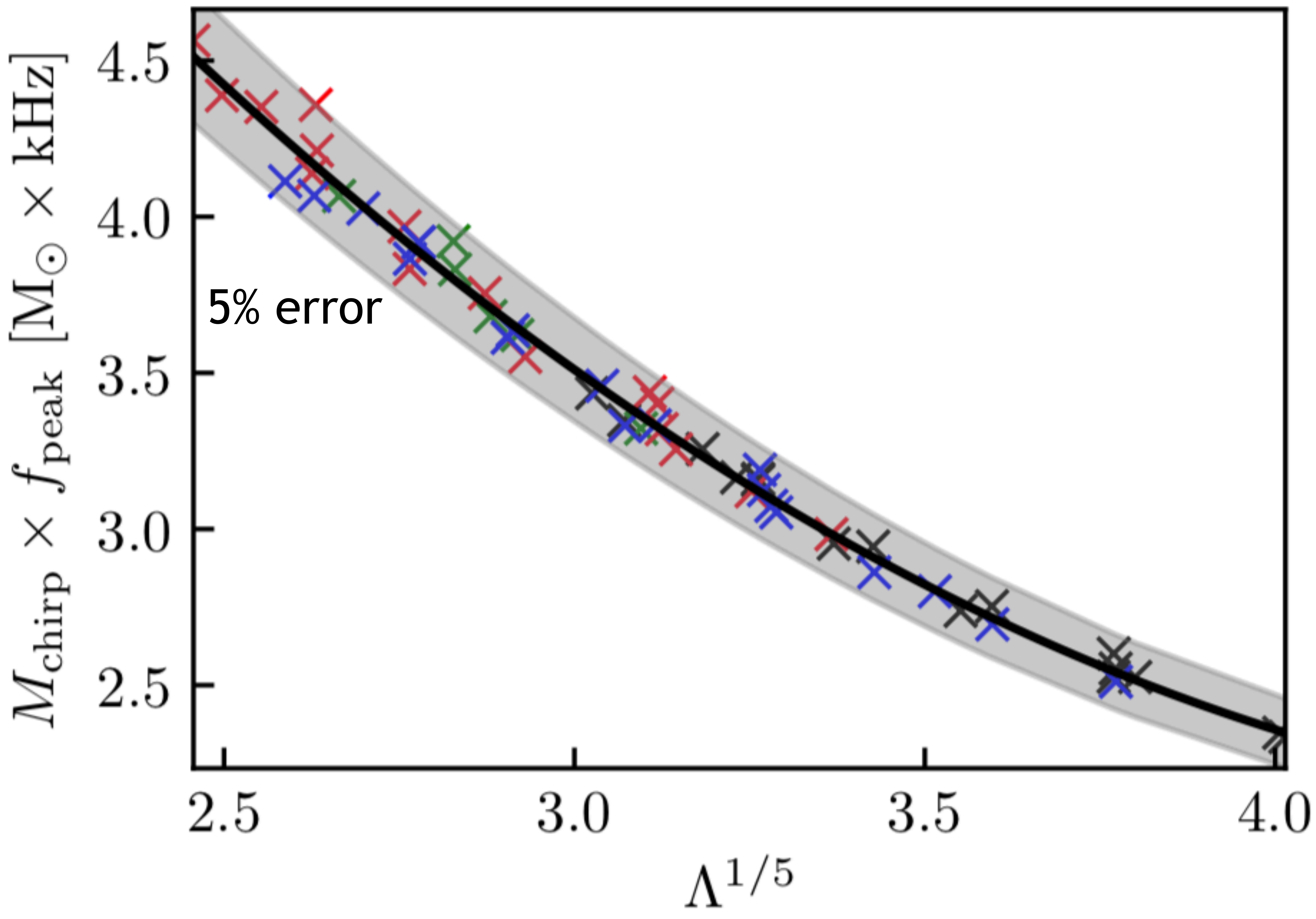

DETECTABILITY OF POST-MERGER PHASE

Single-detector detectability (S/N>5, optimal orientation)

Instrument	$\mathrm{SNR_{full}}$	$\mathrm{SNR_{post}}$	$D_{\rm hor}$ [Mpc]	$\dot{\mathcal{N}}_{\rm det}$ [year^{-1}]
aLIGO	$2.99_{2.37}^{3.86}$	$1.48_{1.13}^{1.86}$	$29.89_{23.76}^{38.57}$	$0.01_{0.01}^{0.03}$
A+	$7.89_{6.25}^{10.16}$	$4.19_{3.26}^{5.35}$	$78.89_{62.52}^{101.67}$	$0.13_{0.10}^{0.20}$
LV	$14.06_{11.16}^{18.13}$	$7.28_{5.64}^{9.30}$	$140.56_{111.60}^{181.29}$	$0.41_{0.21}^{0.88}$
ET-D	$26.65_{20.81}^{34.28}$	$12.16_{9.34}^{15.31}$	$266.52_{208.06}^{342.80}$	$2.81_{1.33}^{5.98}$
CE	$41.50_{32.99}^{53.52}$	$20.52_{15.72}^{25.83}$	$414.62_{329.88}^{535.221}$	$10.59_{5.33}^{22.78}$

Clark, Bauswein, Stergioulas, Shoemaker (2016)

Possible Improvements:

- Network of 5 detectors
- Stacking of several detections
- Improved templates

DETECTABILITY OF POST-MERGER PHASE

Wavelet-based reconstruction algorithm **BayesWave**

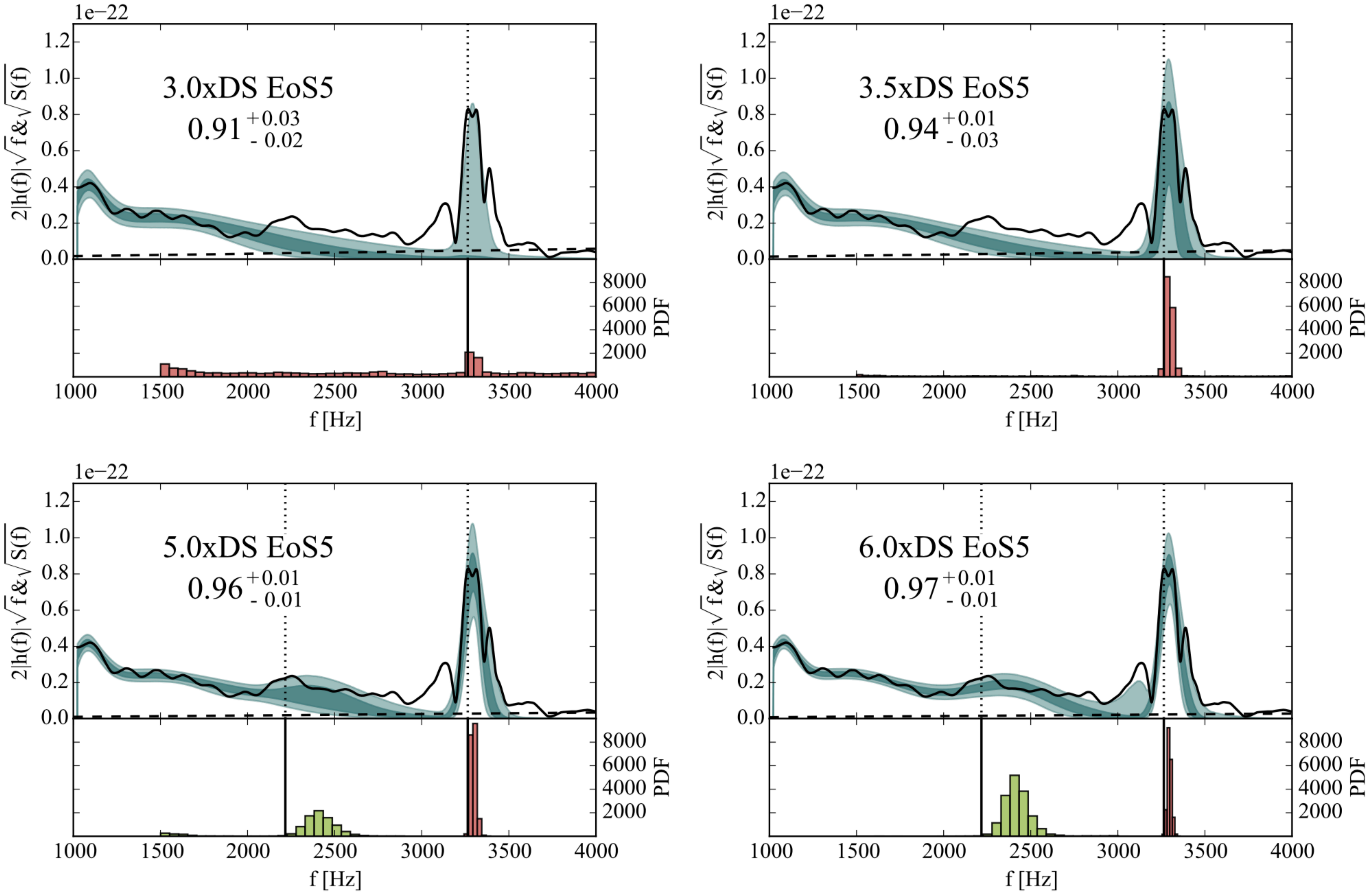

Torres-Rivas, Chatziioannou, Bauswein, Clark (2019)

LOW |T/W| INSTABILITIES IN POST-MERGER REMNANTS

Revival of the m=2 mode at late times, due to a low $|T/W|$ *shear instability*, triggered by *corotation points*.

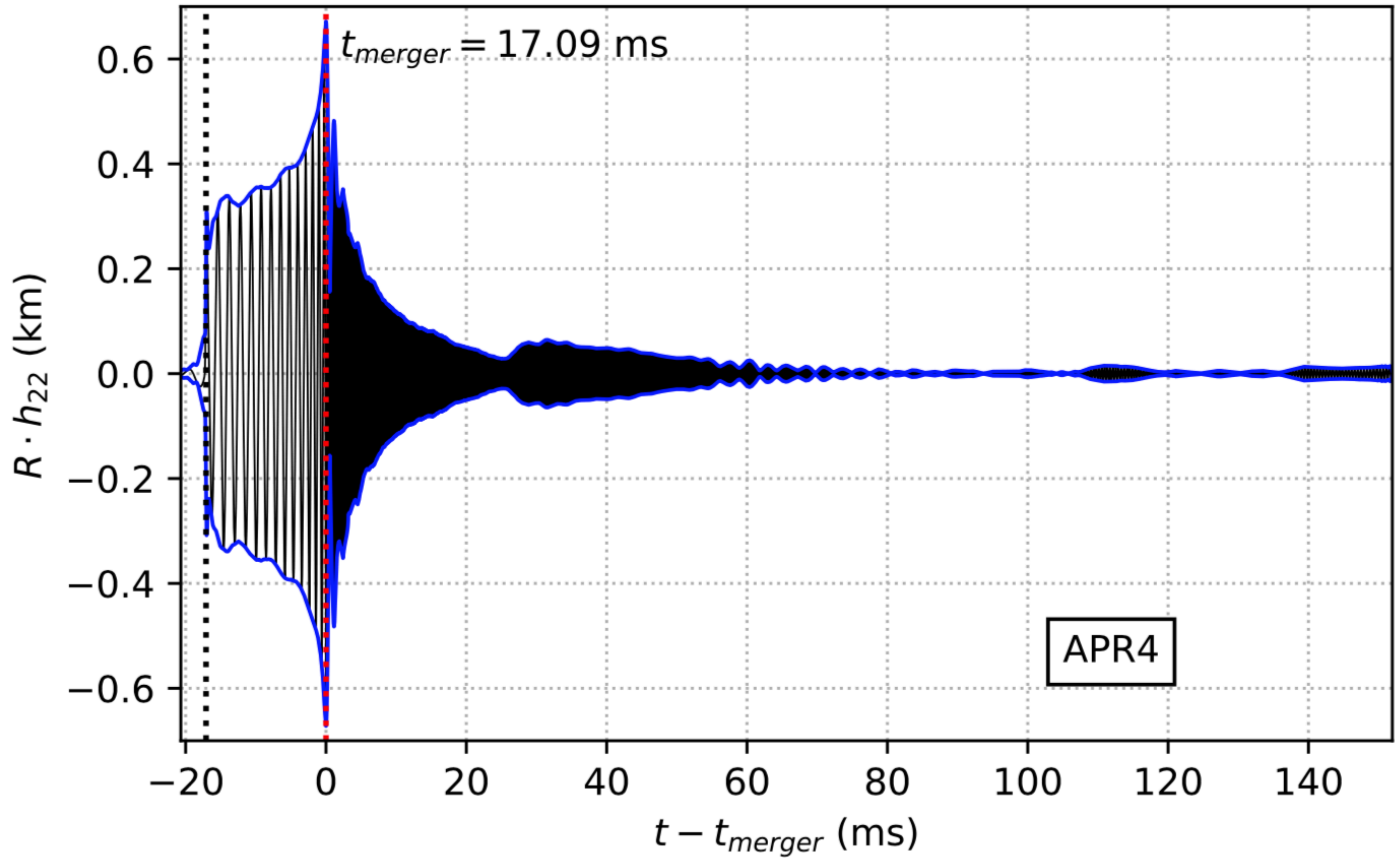

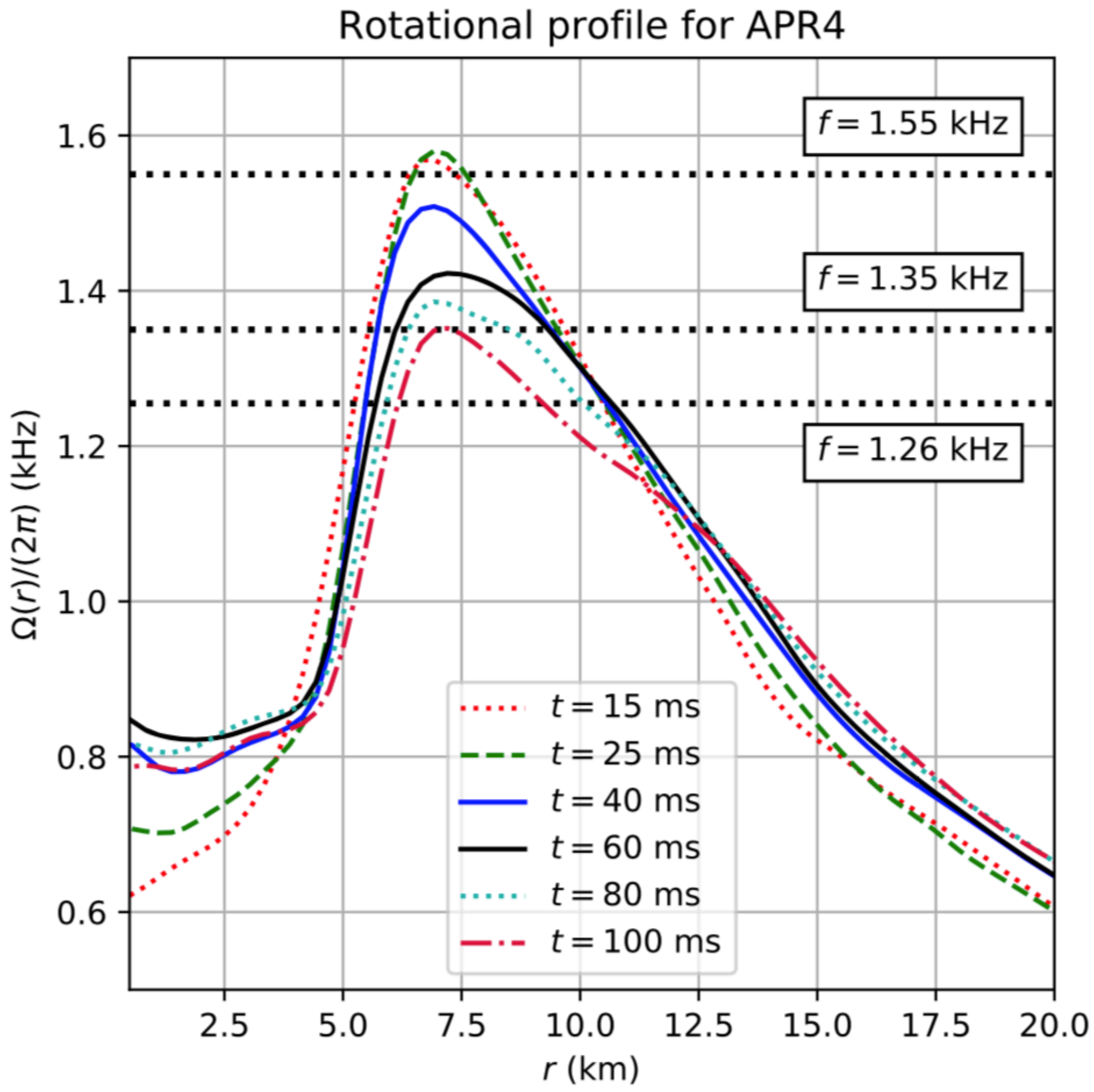

De Pietri et al. (2020)

see also Passamonti, Andersson (2020); Xie et al. (2020)

CONVECTIVE INSTABILITIES AND INERTIAL MODES IN POST–MERGER REMNANTS

At late times, convective instabilities trigger (gravito)-inertial oscillations.

Sign of Schwarzschild discriminant in equatorial plane:

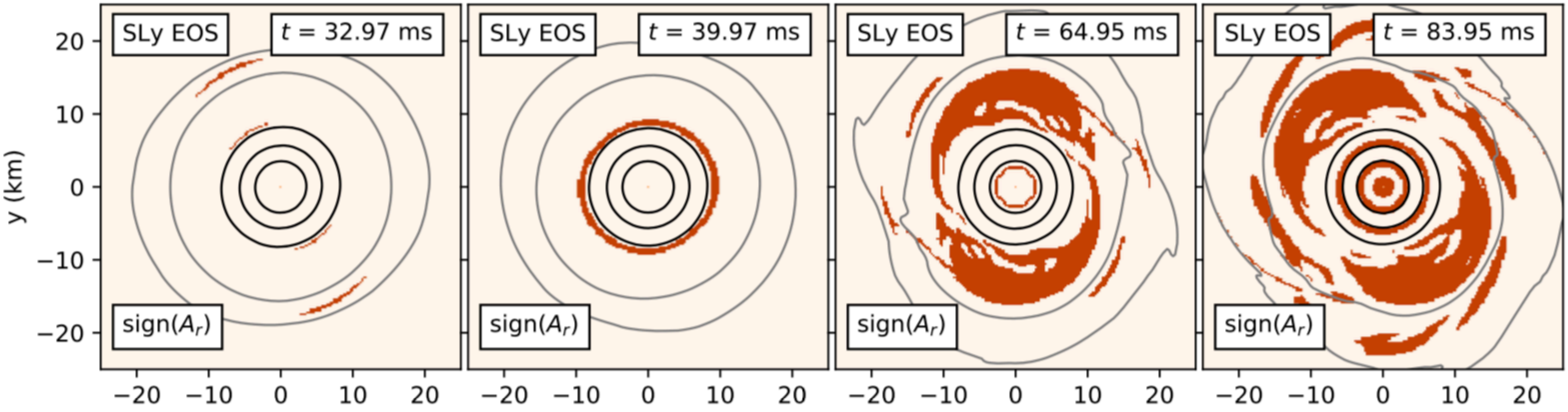

De Pietri et al. (2018) ; De Pietri et al. (2020)

CONVECTIVE INSTABILITIES AND INERTIAL MODES IN POST-MERGER REMNANTS

Potentially detectable with 3G detectors, unless suppressed by strong effective viscosity (e.g. due to MRI).

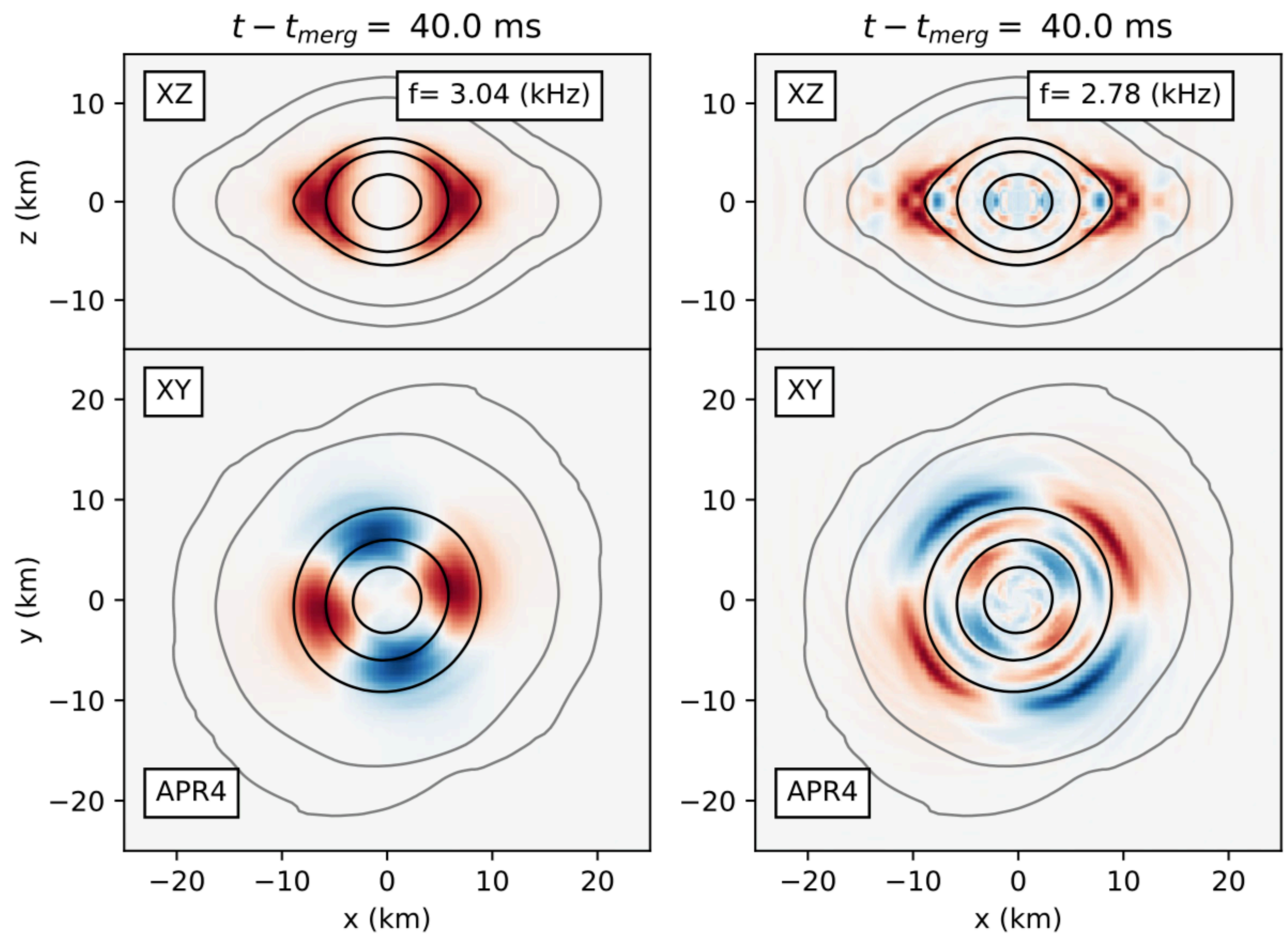

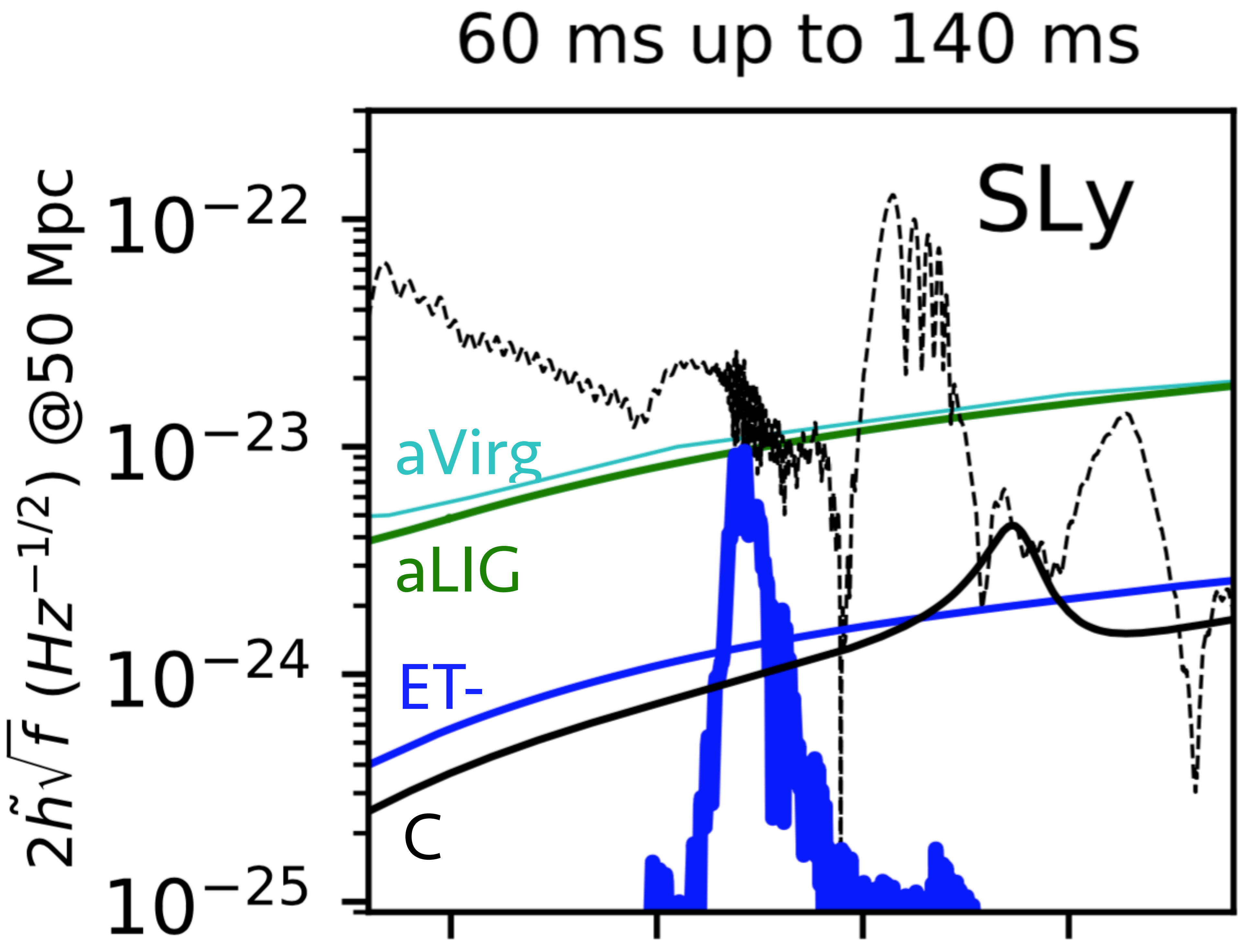

De Pietri et al. (2018) ; De Pietri et al. (2020)

CONCLUSIONS

1) The post-merger phase has rich GW phenomenology and good prospects for constraining EOS

2) The frequency of the main post-merger GW peak shows a tight correlation with the frequency of the fundamental quadrupole oscillation of isolated neutron stars.

3) We construct accurate empirical relations for the threshold mass M_{thres}, including asymmetric binaries.

4) We construct equilibrium models of post-merger remnants with realistic rotation profiles.

5) Using the equilibrium models, we can reproduce the threshold mass to collapse with remarkable accuracy.